

What could go wrong? Discovering and describing failure modes in computer vision

Gabriela Csurka Tyler L. Hayes Diane Larlus Riccardo Volpi

NAVER LABS Europe

<https://europe.naverlabs.com>

Abstract

Deep learning models are effective, yet brittle. Even if carefully trained, their behavior tends to be hard to predict when confronted with out-of-distribution samples. In this work, our goal is to propose a simple yet effective solution to *predict* and *describe* via natural language potential failure modes of computer vision models. Given a pretrained model and a set of samples, our aim is to find sentences that accurately describe the visual conditions in which the model underperforms. In order to study this important topic and foster future research on it, we formalize the problem of Language-Based Error Explainability (LBEE) and propose a set of metrics to evaluate and compare different methods for this task. We propose solutions that operate in a joint vision-and-language embedding space, and can characterize through language descriptions model failures caused, *e.g.*, by objects unseen during training or adverse visual conditions. We experiment with different tasks, such as classification under the presence of dataset bias and semantic segmentation in unseen environments, and show that the proposed methodology isolates nontrivial sentences associated with specific error causes. We hope our work will help practitioners better understand the behavior of models, increasing their overall safety and interpretability.

1. Introduction

The sharp contrast between the ideal conditions found in standard benchmarks and the unpredictable nature of the real world majorly hinders the deployment of computer vision systems in the wild. Despite the most meticulous efforts, samples used to train and validate visual models will only represent a fraction of the diversity that these models will face once deployed. It is thus critical to detect model vulnerabilities and bring them to the user’s attention in an interpretable way [6].

Among research lines that focus on advancing model interpretability, a prominent one is that of *explaining errors made by computer vision models via natural language descriptions*. Different works have addressed the problem of Language-Based Error Explainability (LBEE) before [9, 20, 34, 49, 51]. Yet, none of them proposed ways to quantitatively assess the predicted descriptions, mainly confining them to a qualitative inspection of the model’s error modes. We assert that the LBEE problem requires appropriate metrics, in order to rank methods and track progress in this field. In this paper, we take different steps in this direction through the following contributions: *i)* we provide a rigorous formalization of the LBEE problem, *ii)* we propose a family of methods to tackle it, and *iii)* we introduce different metrics to evaluate performance.

In short, the problem at hand is the following: Given a set of images, denoted by X , a task-specific pre-trained model M_θ , and a large sentence set S , our desired output is a subset of sentences $S^* \subset S$ that describes in plain text the samples from X on which the model M_θ underperforms. To tackle this problem, we propose a simple, yet powerful family of approaches that summarize the visual conditions deemed challenging for a given model via natural language. Our methods rely on uncertainty estimation to distinguish between samples for which the model is more likely to perform well or poorly, and on clustering in a joint vision-and-language embedding space to group together challenging samples associated with specific visual conditions. Operating in this joint representation space allows us to associate sentences to each identified cluster of samples (see illustration in Fig. 1). In order to isolate sentences that are unique to each cluster composed of underperforming samples, we propose different ways to contrast descriptions of the clusters on which the model struggles with the ones on which it performs well (denoted as *hard* and *easy* clusters, respectively).

Our proposed family of approaches is unsupervised and task-agnostic, departing from previous methods which have been specifically designed for classification [9, 20, 51], and often require access to ground-truth or privileged information, such as the types of errors to be

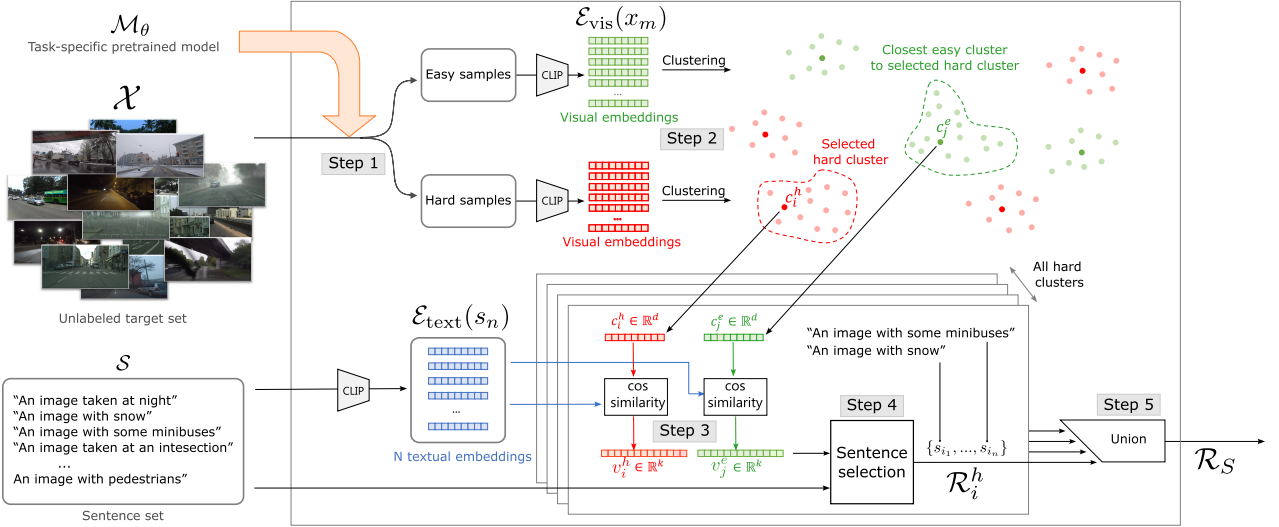


Figure 1: **Overview.** Provided with a pretrained model M_θ , a target image set \mathcal{X} , and a set of sentences \mathcal{S} , the family of solutions we propose for LBEE follows the following steps. In Step 1, images from the target set \mathcal{X} are split into easy and hard samples, based on the model’s confidence. In Step 2, samples are embedded using Open-CLIP and the visual embeddings of each set are clustered (independently). In Step 3, for each hard and easy cluster we compute the cosine similarities between the textual embeddings of candidate sentences and the cluster prototypes. We also assign the closest easy prototype to each hard prototype. Step 4 performs sentence selection for that hard cluster, based on these sentence-prototype similarities. Step 5 aggregates the cluster-specific sentence sets to produce the output.

discovered [9, 51]. To assess how well these methods find suitable failure explanations, we introduce metrics specifically designed for LBEE capturing whether or not the sentences satisfactorily explain reasons for failure, and how well the produced sentences describe the images within each error mode.

While the need to provide the sentence set \mathcal{S} is a practical limitation of our methods, it plays a crucial role as it allows 1) defining a more generic ground-truth (GT) for evaluation that goes beyond human-in-the-loop qualitative assessment, 2) finding more subtle explanations than clear test set’s biases (e.g. “waterbirds in land” [26], “blonde males” in CelebA [28] or human-implanted biases in NICO++ [9, 51]), 3) performing a fair and quantitative comparisons of different methods, and 4) avoiding the need to involve the assessment with a large language model (e.g., as in [8]).

In summary, the contributions of our paper are: *i)* formalizing the LBEE problem (Sec. 3); *ii)* proposing a family of methods to tackle it (Sec. 4); *iii)* introducing different metrics to evaluate performance (Sec. 5); *iv)* showing the effectiveness of our proposed solutions through extensive experiments, focusing on both classification and semantic segmentation tasks (Sec. 6).

2. Related work

Automated error discovery. Recently, methods to assess errors made by machine learning models have shifted from human-in-the-loop approaches [5, 10, 19, 42, 50] to automatic detection of consistent model failure modes [9, 20, 34, 49, 51].

In particular, Eyuboglu *et al.* [9, 51] propose to learn a mixture model to partition the data according to classification errors related to spurious correlations. Jain *et al.* [20] characterize model failures as directions in a latent space learned by SVMs. Kim *et al.* [23] identify biases by analyzing captions from misclassified images with a Vision-Language Model (VLM) and rank the keywords from the captions using CLIP [32]. Wiles *et al.* [49] use conditional text-to-image diffusion models to generate synthetic images that are grouped based on how the model misclassifies them. Rezaei *et al.* [34] extract human-understandable concepts (tags) with VLMs and examine the model’s behavior conditioning on the presence or absence of the combination of those tags. Also Metzen *et al.* [30] rely on text-to-image models: by encoding specific information in the prompt, they synthesize images from the combinatorially large set of data sub-populations, and run tests to find out on which ones the model underperforms. Finally, a recent work proposes methods to describe differences between two image sets [8]. While this method could be applied

to LBEE, the proposed evaluation based on GPT-4 can only assess whether the difference between the sets is correct but not whether this difference is related or not to model failure.

In contrast with the above works, our method only require encoding the images and the textual explanations in a shared visual-textual space such as CLIP, where we rely on simple arithmetic operations among clusters to characterize them via natural language. Our solutions seamlessly apply to arbitrary image task, and indeed we port this line of work to semantic segmentation for the first time. Differently from previous work on this topic, we also provide a rigorous formalization of the LBEE problem, with ad hoc metrics.

Explainability. There is a growing body of work connecting explainable AI and CV. Several focus on producing visual explanations visualizing image regions that contribute most to model failures [35,40,44,53]. A few works aim at generating counterfactual explanations [11,16,18], identifying small image edits that cause the model to fail. More recently, diffusion models have been used to this end [2,21,46]. In contrast to these methods which only explain failures on a particular image, our aim is to provide explanations of the model’s overall behavior on an entire image set, in order to uncover consistent error patterns and major weaknesses under particular conditions. Furthermore, we rely on natural language as a more interpretable interface.

Another body of work tackles interpretability by providing short text descriptions to describe why a model has produced some output [13,15,22,38]. Such methods are related to our work, in that we are also interested in generating language descriptions for model behaviors; yet, we are interested in *failure modes*, not in the general rationale behind a prediction.

3. Language-Based Error Explainability

We can define the LBEE problem as automatically finding and describing potential errors from a model based on its performance on a given dataset. Formally, let \mathcal{M}_θ be a computer vision model parameterized by θ , for an arbitrary computer vision task, such as classification or segmentation. Let $\mathcal{X} = \{\mathbf{x}_i\}_{i=1}^M$ be a set of images sampled from an arbitrary target distribution, and let $\omega_\theta^{\text{avg}}$ be the average performance of the model on such data. Finally, let $\mathcal{S} = \{s_n\}_{n=1}^N$ be a broad and generic set of sentences that describe various visual elements and conditions, which can be either manually defined or generated with a large language model (LLM)—see Appendix C.

Problem formulation. Given a target set \mathcal{X} , our goal

is to find a set of sentences $\mathcal{R}_\mathcal{S} \subset \mathcal{S}$ describing any likely failure causes for the model \mathcal{M}_θ with respect to images from \mathcal{X} —such as unseen objects, visual conditions never encountered during training, or errors of any other nature. Intuitively, each selected sentence in $\mathcal{R}_\mathcal{S}$ should describe elements present in images on which the models fails and not in those in which the model succeeds.

Letting $\omega_\theta^{s_n}$ be the average performance of the model on images for which the sentence s_n is relevant, we determine that such sentence is *describing a failure mode* if the difference between the global average $\omega_\theta^{\text{avg}}$ (average over all images in \mathcal{X}) and $\omega_\theta^{s_n}$ is larger than a threshold β , namely a predefined margin. The desired output \mathcal{S}_β^* , used to evaluate the performance of the methods, is the collection of all of these sentences

$$\mathcal{S}_\beta^* = \{s_n \in \mathcal{S} \mid \omega_\theta^{s_n} < \omega_\theta^{\text{avg}} - \beta\} , \quad (1)$$

Note that β allows the user to set an arbitrary severity level for the error descriptions, *i.e.*, a higher β restricts the desired set \mathcal{S}_β^* to more challenging sentences. We provide more details in Appendix C.2.

Relation with prior art. To conclude this section, we position the formulation introduced above with the ones tackled by related works [9,20,51].

One core difference is that these methods limit their problem formulation to the classification task, while we do not make any assumption related to the nature of the task at hand. Furthermore, in [20] they analyze errors *per class*, and in [9,51] assume access to ground truth or prior knowledge about the error types to look for (*e.g.*, bias-conflicting sub-populations or context). In contrast to the above works, we do not use any knowledge about errors prior to evaluation and neither assume, in general, access to class information. Finally, while in prior works the language-based descriptions are part of the proposed methodology, they are not part of the problem formulation and they are not quantitatively evaluated. Instead, we treat the language-based description of errors made by computer vision models as the problem itself, providing means to evaluate them.

4. A family of approaches to solve LBEE

We propose a family of simple, unsupervised and task agnostic approaches to tackle the LBEE problem. Our solutions rely on two key elements: *i)* a joint vision-and-language space \mathcal{F} , for which we use Open-CLIP [17], and *ii)* the sentence set \mathcal{S} introduced in the previous section, assumed to be large enough to describe images from the target set and to contain potentially relevant reasons for model failure (see Appendix C).

We recall that the problem at hand is the following: Given a set of images, denoted by \mathcal{X} , a task-specific pretrained model \mathcal{M}_θ , and a large sentence set \mathcal{S} , we want to select the subset from \mathcal{S} that describes the samples from \mathcal{X} on which the model \mathcal{M}_θ underperforms. Our proposed solution is illustrated in Fig. 1 and follows the steps detailed below.

Step 1: Splitting the target set into easy and hard subsets. Given the model \mathcal{M}_θ and a confidence measure φ_θ , we define two thresholds t_φ^h and t_φ^e and split the target set \mathcal{X} into three sets: an easy one $\mathcal{X}^e = \{\mathbf{x}_i \in \mathcal{X} | \varphi_\theta(\mathbf{x}_i) > t_\varphi^e\}$, a hard one $\mathcal{X}^h = \{\mathbf{x}_i \in \mathcal{X} | \varphi_\theta(\mathbf{x}_i) < t_\varphi^h\}$, and, if $t_\varphi^e > t_\varphi^h$, a neutral set with the remaining images. If ground truth for the target set is available, we can instead use the model’s performance to split the data.

Step 2: Clustering easy and hard subsets. Let us denote by \mathcal{E}_{vis} and \mathcal{E}_{txt} the visual and text encoders mapping images and sentences into the joint space \mathcal{F} , respectively. Let $\Phi = \{\mathcal{E}_{\text{vis}}(\mathbf{x}_m)\}_{m=1}^M$ be the set of visual representations of images in \mathcal{X} and let Φ^h and Φ^e be the set of representations associated with hard and easy samples, respectively. We cluster the samples in Φ^h and Φ^e independently, using an arbitrary clustering method¹ and represent each cluster by its centroid, referred also as its *prototype*. We compute it as the average of the embeddings of the samples in the cluster. Let $C^h = \{\mathbf{c}_i^h\}_{i=1}^{|C^h|}$ and $C^e = \{\mathbf{c}_j^e\}_{j=1}^{|C^e|}$ be the set of prototypes associated with hard and easy samples, respectively. In the remainder of the paper, we will use \mathbf{c}_i^h and \mathbf{c}_j^e to indistinctly refer to the clusters or to their prototypes.

Step 3. Matching sentences with prototypes. Let us denote by $\mathbf{s}_n = \mathcal{E}_{\text{txt}}(s_n)$ the textual embeddings of the sentences s_n . These embeddings lie in the same joint embedding space as the images and, in turn, as the prototypes \mathbf{c}_i^e and \mathbf{c}_i^h . Therefore, for each prototype \mathbf{c} (easy or hard) we can compute the cosine similarity (i.e., the dot product between L2-normalized representations) to each textual embedding \mathbf{s}_n . We can store these similarities into a vector $\mathbf{v} \in \mathbb{R}^N$, where the n^{th} element of this vector is $\langle \mathbf{c}, \mathbf{s}_n \rangle$. This allows us to characterize each cluster in terms of its semantic similarity with the sentences in \mathcal{S} .

Step 4: Retrieving sentences for hard prototypes. Here, we look for a set of peculiar sentences for each hard cluster. To select relevant sentences for a given cluster (easy or hard), we simply rank the sentences by their similarity to the cluster center (by ranking the elements of the vectors \mathbf{v}_j^e and \mathbf{v}_i^h). Then we either retain

the top ranked sentences or all sentences with a corresponding value in \mathbf{v} above a predefined threshold τ . We denote the set of retained sentences for \mathbf{c}_i^h and \mathbf{c}_j^e by \mathcal{S}_i^h and \mathcal{S}_j^e , respectively. While \mathcal{S}_i^h effectively describes images within \mathbf{c}_i^h , not all sentences will point to failure reasons. We need to find sentences describing the visual features that make the cluster *hard*. We propose therefore to contrast the hard cluster with its closest easy cluster: its proximity in \mathcal{F} implies content similarity, hence, contrasting allows isolating the attributes that characterize the hard cluster specifically, and not the easy one.

Let $\mathbf{c}_j^e \in C^e$ be the closest easy prototype to $\mathbf{c}_i^h \in C^h$ based on their distance in \mathcal{F} . In the following, we propose three different methods to isolate sentences that are peculiar to the hard cluster \mathbf{c}_i^h . For a fair and more straightforward comparison between different methods, we fix the number of sentences retained for each cluster and for each method to a predefined K , i.e. $|\mathcal{R}_i^h| = K$, where \mathcal{R}_i^h is the sentence set retained by a method for the hard cluster \mathbf{c}_i^h .

SetDiff: Sentence set differences. Given a pair of clusters $(\mathbf{c}_i^h, \mathbf{c}_j^e)$, we first select relevant sentences for both— \mathcal{S}_i^h and \mathcal{S}_j^e —and then remove from \mathcal{S}_i^h the sentences that are present in \mathcal{S}_j^e , yielding $\mathcal{R}_i^h = \mathcal{S}_i^h \setminus \mathcal{S}_j^e$. Since this approach does not guarantee that $|\mathcal{R}_i^h| = K$, we fill \mathcal{S}_j^e with sentences corresponding to values in \mathbf{v}_j^e above a threshold² τ and build \mathcal{R}_i^h with the K most similar sentences to \mathbf{c}_i^h that are not in \mathcal{S}_j^e .

PDiff: Prototype difference. Assuming that higher scores in the element-wise difference between the similarity vectors $\mathbf{d}_i^h = \mathbf{v}_i^h - \mathbf{v}_j^e$ better describe the hard clusters than the easy ones³, we can rank \mathbf{d}_i^h and retain the sentences corresponding to the top K values. We denote this set by \mathcal{S}_i^d and define $\mathcal{R}_i^h = \mathcal{S}_i^d$.

FPDiff: Filtered PDiff. A drawback of **PDiff** is that it does not guarantee that the selected sentences accurately describe the hard cluster. A remedy to this is only retaining sentences that have high similarity to the prototype \mathbf{c}_i^h , namely sentences in \mathcal{S}_i^d that are also in \mathcal{S}_i^h . We define $\mathcal{R}_i^h = \mathcal{S}_i^h \cap \mathcal{S}_i^d$. Also here, to guarantee that $|\mathcal{R}_i^h| = K$, we fill \mathcal{S}_i^h with sentences corresponding to values in \mathbf{v}_i^h above a threshold τ and build \mathcal{R}_i^h with the top K sentences having the highest values in \mathbf{d}_i^h that are also in \mathcal{S}_i^h .

¹We use Agglomerative Clustering with Ward-linkage [48] in our experiments.

²We set $\tau = 0.25$ based on the observation that the average similarity between our sentence sets and image sets is around 0.17, due to the well-known modality gap [25].

³This, up to some normalization, is equivalent to first consider the prototype differences and then compute the similarity between each sentence s_n and \mathbf{d}_i^h .

TopS. We also include a baseline called **TopS**, describing the hard clusters without any contrasting, by selecting the top K ranked sentences from \mathcal{S}_i^h ($\mathcal{R}_i^h = \mathcal{S}_i^h$).

Step 5: Producing the final output. The final set of sentences that describe potential reasons for failure for the whole dataset is the union of all the sentence sets retained for all the hard clusters, namely

$$\mathcal{R}_S = \bigcup_{i=1}^{|\mathcal{C}^h|} \mathcal{R}_i^h. \quad (2)$$

We conclude by positioning these methods with respect to prior works.

Relations with prior art. As mentioned in Sec. 3, prior art [9, 51] describes a problem formulation that does not perfectly align with ours. Yet, their approaches proposed to assign explanations to predicted error modes can be related to some of the methods we propose above. DOMINO [9], which associates sentences based on average CLIP embedding from which the average class representative is extracted, is closely related to **PDiff**: when we analyze the errors per class (see Sec. 6), this version of our method can be interpreted as a variant of DOMINO in which the class prototype is replaced with the closest easy prototype. FACTS [51] relies on a captioning tool [31] to assign a single tag to each partition without contrasting, hence, it is mostly related to **TopS**.

5. Evaluation metrics for LBEE

Our third contribution is a set of metrics to evaluate predicted language explanations by LBEE methods, which can retrieve error-related sentences without any supervision for an arbitrary visual task. Concretely, given the output of a method, namely the set of sentences $\mathcal{R}_S \subset \mathcal{S}$, we need to assess *i) whether these sentences actually point to reasons for model failure*, *ii) how well the retrieved sentences characterize the image set assigned to the cluster*, and *iii) how well the predicted sentence set \mathcal{R}_S covers the set of potential explanations given by \mathcal{S}_β^** . We propose metrics that allow measuring a method’s performance in these dimensions.

i) Average Hardness Ratio (AHR). Our main goal is retrieving sentences s_n that *point to reasons for model failure*, i.e., $s_n \in \mathcal{S}_\beta^*$. This means that the hardness score of the sentence $\omega_\theta^{s_n}$ —formally defined in Eq. (8), Appendix C.2—satisfies the condition $\omega_\theta^{s_n} < \omega_\theta^{avg} - \beta$. The lower this value is, the more the sentence is correlated with model failure.

We define the Hardness Ratio (HR) for a given cluster as the ratio of sentences among the retrieved ones in

\mathcal{R}_i^h (see Sec. 4) for which the above condition holds

$$HR_i = \frac{|\mathcal{R}_i^h \cap \mathcal{S}_\beta^*|}{|\mathcal{R}_i^h|}, \quad (3)$$

and we define the AHR as the average across all clusters

$$AHR = \frac{1}{|\mathcal{C}^h|} \sum_{i=1}^{|\mathcal{C}^h|} HR_i.$$

ii) Average Coverage Ratio (ACR). Next, we introduce a metric to assess the *coverage* of the sentences associated with the hard clusters, i.e. the ratio of images in the cluster for which the retrieved sentence holds. Intuitively this shows how well a sentence $s_n \in \mathcal{R}_i^h$ characterizes a hard cluster \mathcal{C}_i^h . CR_i is the mean of these ratios taken over the sentences retained in \mathcal{R}_i^h . Formally,

$$CR_i = \frac{1}{|\mathcal{R}_i^h|} \sum_{s_n \in \mathcal{R}_i^h} \frac{1}{|\mathcal{C}_i^h|} \sum_{\mathbf{x}_m \in \mathcal{C}_i^h} \Gamma(\mathbf{x}_m, s_n), \quad (4)$$

where $\Gamma(.,.)$ is a binary operator that, taking in input an image and a sentence, outputs 1 if the sentence s_n is relevant for the image \mathbf{x}_m and zero otherwise (see Appendix C.2 for details). To obtain the final ACR value, we simply average CR_i across all clusters, namely

$$ACR = \frac{1}{|\mathcal{C}^h|} \sum_{i=1}^{|\mathcal{C}^h|} CR_i.$$

iii) \mathcal{R}_S vs. \mathcal{S}_β^* . To assess if the union of the retained sentences \mathcal{R}_S (defined in Eq. (2)) accurately covers the potential errors represented by $\mathcal{S}_\beta^* \subset \mathcal{S}$, we compute the True Positive Rate (TPR) of the retrieved sentences and the Jaccard Index (JI) between the two sets

$$TPR = \frac{|\mathcal{R}_S \cap \mathcal{S}_\beta^*|}{|\mathcal{S}_\beta^*|} \quad \text{and} \quad JI = \frac{|\mathcal{R}_S \cap \mathcal{S}_\beta^*|}{|\mathcal{R}_S \cup \mathcal{S}_\beta^*|}. \quad (5)$$

TPR indicates how well a method covers the ground-truth explanations, while JI measures the overall coverage, also taking into account false positives.

6. Experiments

Experimental setup. We tackle three tasks: semantic segmentation of urban scenes, classification under the presence of spuriously correlated data, and large-scale ImageNet classification. For the first, we consider a ConvNeXt [29] segmentation model trained on Cityscapes [3] and test on three challenging datasets: WD2 [52], IDD [45] and ACDC [37]. For the second task we train ResNet50 image classification models on different spuriously correlated data derived from

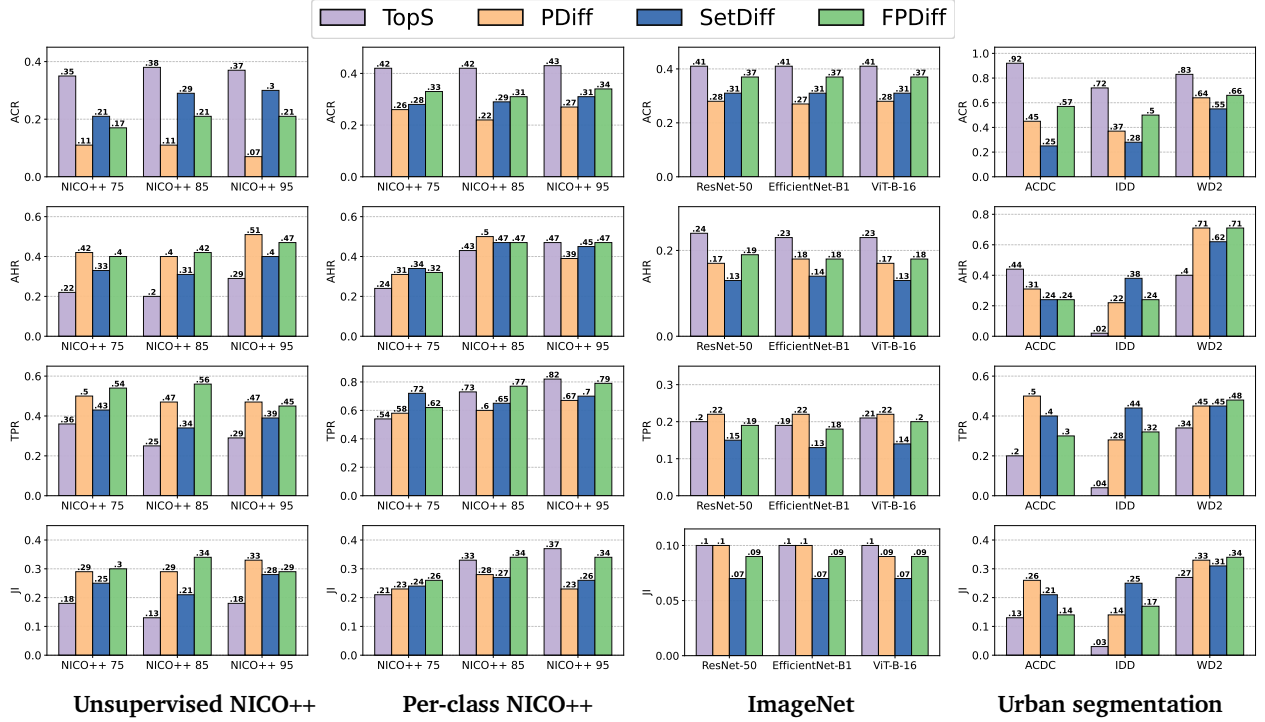


Figure 2: **Numerical results (all datasets).** From top to bottom: ACR, AHR, TPR and JI scores on NICO++ unsupervised and supervised per-class (first and second column, respectively), ImageNet per-class (third column) and Urban Scene Segmentation (last column).

NICO++ and demonstrate how the proposed approaches can be used for understanding model failures due to such subtle biases [14, 55]. We consider two cases, an unsupervised case where the full set is split with class prediction entropy and a supervised one, where following [9, 51] we analyze the performance on each class separately. In the latter case we use the class prediction to split the data into easy and hard sets and, in addition to evaluating LBEE, we compare our simple split-and-cluster partitioning to the more complex partitioning methods from [9, 51], using their evaluation protocol (see in Appendix B). Finally, to showcase the scalability of our approaches, we analyze different pre-trained architectures on the ImageNet 1K validation set, focusing on the top-1 classification performance and seeking for explanations for each class individually. We provide details about each task, related models and the datasets in Appendix A.

Default design choices. We use Open-CLIP [17] as vision-and-language embedding space. S is a User-defined sentence set in the case of urban scene segmentation and ImageNet and GT-based for NICO++ (see details in Appendix C.1). To generate the ground-truth sentence set S_β^* containing the sentences with valid *hardness score* (see Appendix C.2), we set $\beta = .2 * \omega_\theta^{\text{std}}$ with $\omega_\theta^{\text{std}}$ being the standard deviation of ω_θ computed

over X . We set the number of hard clusters to $C = 15$ for large datasets and $C = 5$ for the per-class data analyses. We use the same number of clusters for the easy set ($|C^h| = |C^e| = C$). To split the data we use the output entropy in the unsupervised cases and class probability or ranking in the per-class case (see details in Appendix D). We retain three sentences for each cluster ($K = 3$).

In the following, we show numerical results and illustrate them with some qualitative examples. We report in-depth analyses for the different datasets, also concerning the sensitivity to crucial hyper-parameters.

6.1. Results

In Figs. 3, 5, 7, 9 and 11 we report qualitative results, showing the sentences selected by our methods for various hard clusters. In all cases, each row represents a hard cluster, and at the bottom we report the three sentences provided by the different methods.

Focusing, e.g., on Figs. 3, 5 and 7 (urban segmentation on ACDC, IDD and WD2, respectively) we can see that our methods can successfully isolate the main reasons for the clusters to be *hard*, for example difficult visual conditions (*rainy/foggy weather* or *image taken at night*) or the presence of elements unseen during training such as *tunnels*, *mud* or *light reflections*). Indeed, such elements can represent real challenges for a model trained

Table 1: **Examples of sentences from the User-defined sentence set S .** For each sentence we show if it belongs to S_β^* and to \mathcal{R}_S for **TopS (TS)**, **PDiff (PD)**, **SetDiff (SD)** and **FPDiff (FP)** for the datasets WD2, IDD and ACDC. “✓” means $s_n \in S_\beta^*$ and “✗” means $s_n \notin S_\beta^*$ —namely, the hardness score of s_n is below the required level. For the methods, “+”/“+” indicate that the sentence is in \mathcal{R}_S , where “+” means true positive (i.e., the sentence is also in S_β^*) while “+” means false positive. An empty space indicates that the sentence is not in the corresponding \mathcal{R}_S .

Sentences (An image ...)	WD2					IDD					ACDC				
	S_β^*	TS	PD	SD	FP	S_β^*	TS	PD	SD	FP	S_β^*	TS	PD	SD	FP
“taken at night”	✓	+	+	+	+	✓		+	+	+	✓	+			
“taken in the evening”	✓		+	+	+	✓		+		+	✓	+			
“taken at dusk”	✓		+	+	+	✓		+	+	+	✓				
“taken in a foggy weather”	✓			+		✓					✗	+	+	+	+
“taken in a rainy weather”	✓	+	+		+	✓					✗	+	+		+
“taken in a snowy weather”	✓		+	+	+	✗					✗	+			
“taken in a dull weather”	✓	+	+	+	+	✗					✗	+	+	+	+
“with reflection on the road”	✓	+	+	+	+	✓			+		✓				+
“with shadows on the road”	✗				+	✗			+		✓			+	
“with water on the road”	✓	+				✗					✗			+	+
“with mud on the road”	✗			+	+	✗		+	+		✗				
“with obstacle on the road”	✓	+			+	✗	+				✗				
“with road barrier on the road”	✗			+		✗			+	+	✓	+	+	+	+
“with rail track on the road”	✗					✓			+	+	✓	+	+	+	+
“with rocks on the road”	✗			+	+	✗					✗				
“showing a highway scene”	✗			+		✗			+	+	✗	+	+	+	+
“showing an industrial scene”	✓					✓					✗				
“showing construction site”	✗					✓		+	+	+	✗		+	+	
“showing sub-urban scene”	✗	+		+		✗	+			+	✓				
“with rickshaw on the road”	✗	+	+	+	+	✗	+	+		+	✓		+		
“with motorbike on the road”	✗		+		+	✗				+	✓				+
“with vehicle on the road”	✗	+				✗	+				✗	+	+	+	+
“with tram on the road”	✗					✗			+		✗	+	+		+
“with jeep on the road”	✗	+		+	+	✗					✗				
“with animal on the road”	✗			+	+	✓			+	+	✗				
“with people on the road”	✗	+			+	✗	+			+	✗		+		
“with crowded foreground”	✗					✗		+	+	+	✗				
“with motion blur”	✓	+	+		+	✓			+	+	✓		+		
“with underexposure”	✗			+	+	✗					✓			+	
“with low contrast”	✓					✗			+	+	✗			+	
“of a tunnel”	✓	+	+	+	+	✓		+			✓	+	+	+	+
“of fences”	✗					✗		+			✓		+		
“of guard-rail”	✗					✗					✗		+	+	+
“of a traffic jam”	✓					✓	+	+		+	✗				
“of traffic lights”	✓					✓					✗		+		
“of a parking”	✗		+			✓		+	+	+	✗		+		

on Cityscapes, as observed also, e.g., in [4].

With our methods, the user can easily asses the potential failures at a glance, instead of inspecting the hundreds of images contained in the above clusters. They could easily rank the images in the cluster for each selected sentence for the visual inspection based on the corresponding Open-CLIP similarity scores. Such information can be further used for different down-stream tasks, for example helping the user to select which new samples to annotate [33, 41].

In Fig. 2, we provide numerical results for the different methods, tasks and datasets, using the metrics introduced in Sec. 5 and the default setting and hyperparameters detailed above. First, we observe that **TopS**

is the best performing method in terms of ACR scores. This is not surprising, since sentences closest to the prototype have obviously the highest coverage. Yet, these sentences are not necessarily pointing to error explanations—indeed, see the low AHR scores in some cases, with IDD being the most dramatic one (right-most column, third panel). Concerning the metrics related to the failure explanations (AHR/TPR/JI), in both NICO++ scenarios, where we have ground truth relevance scores, and on WD2 **FPDiff** performs best or close to it. It performs worse on ACDC and IDD: there is no clear winner among the proposed methods in these two datasets, since the higher performance of **PDiff** and **SetDiff** in terms of TPR and JI comes at the price of a lower ACR.



Figure 3: Two hard clusters in ACDC explained by different methods. We illustrate a few example images from the cluster and below the three sentences retained by different methods for it.

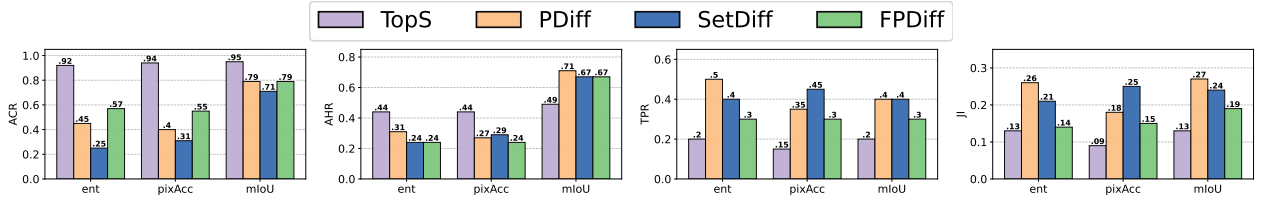


Figure 4: **Unsupervised and supervised splitting (ACDC)**. Results of different metrics (from left to right ACR, AHR, TPR and JI) on the ACDC dataset when the split is done with entropy, pixel accuracy and the mIoU.

In the following, we provide more in-depth analysis focusing on the different datasets.

6.1.1 ACDC

To recap, we test models trained on Cityscapes (daylight and clear weather) on ACDC, which contains samples recorded under various weather and daylight conditions. Results in Fig. 2 show that the best AHR performance is obtained with **TopS**, but also that this method is the worst performing one in terms of TPR and JI. For what concerns the latter metrics, **PDiff** shines as the best performing method. To shed light on these results, we complement them with Tab. 1 (and with the more detailed Tab. 5) showing sentences from the sentence set S that are either in S_{β}^* or in any \mathcal{R}_S , namely the ground truth set of hard sentences and the ones retrieved by our methods, respectively.

From these results we can make the following observations. *i)* The main advantage of **TopS** comes from retrieving the sentences related to images taken at night or in the evening. *ii)* The other methods fail in retrieving these sentences because the closest easy clusters also contain night or evening images. *iii)* On the other hand, these methods often select sentences referring to “fog”, or “rain” (see e.g. Fig. 3) that are indeed valid

characteristics of the images in the cluster, but yet these conditions do not affect sufficiently the model to have a hardness score that satisfies the condition $\omega_{\theta}^{s_n} < \omega_{\theta}^{\text{avg}} - \beta$.

Varying the easy/hard splitting strategy. In order to evaluate the effectiveness of the entropy as a metric to split datasets into easy and hard partitions, in Fig. 4 we compare the results obtained by splitting the ACDC set with entropy *versus* using metrics that rely on annotated samples, namely the pixel accuracy (average of correctly predicted pixels) or mIoU.

We can observe that while using the GT mIoU improved significantly the ACR and AHR scores (averaged over all clusters), globally the TPR and JI changed only slightly. This suggests that, in general, the sentences retained by **PDiff**, **FPDiff** and **SetDiff** have better coverage in the cluster (higher ACR) and retain more often a hardness score that satisfies the required constraint. The TPR and JI scores are comparable across splitting strategy. By analyzing the sentences retrieved in each setting, we discovered that with GT mIoU the contrastive methods are able to recover sentences such as “taken at night”, “taken in the evening” and “taken at dusk”, but fail in retrieving sentences such as “with road barrier”/“with rail track on the road” and “with motion blur”/“with underexposure”, namely sentences that were retrieved

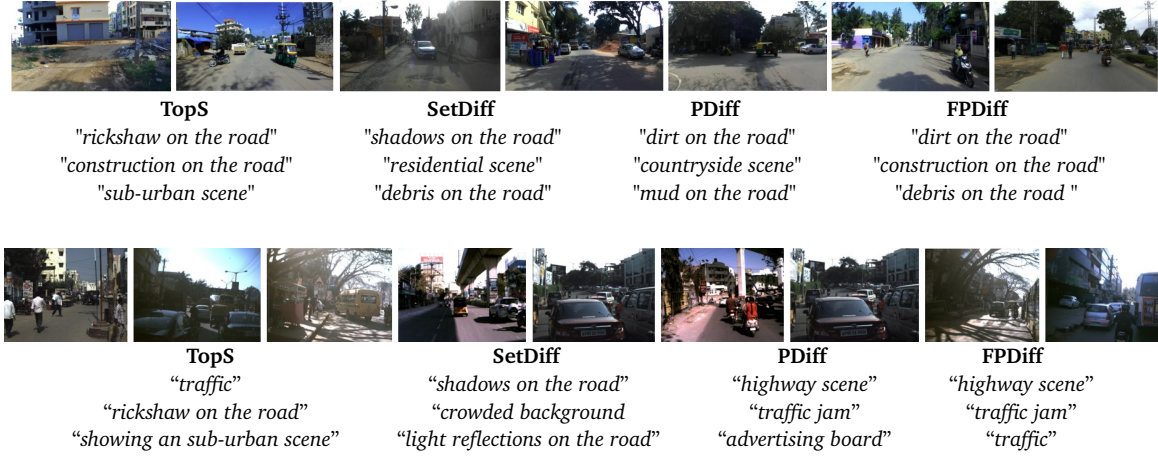


Figure 5: Two hard clusters from IDD explained by different methods. We illustrate a few example images from the cluster and below the three sentences retained by different methods for it.

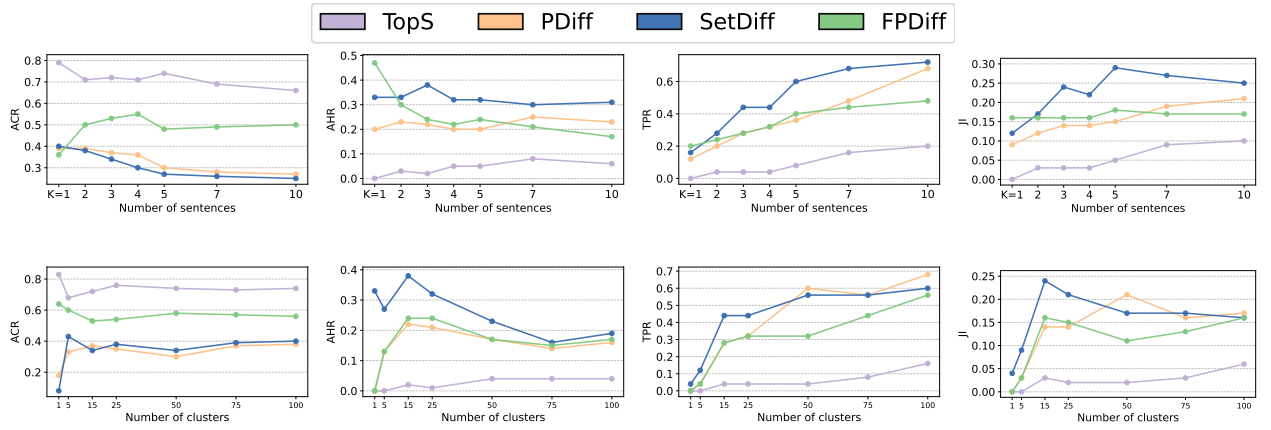


Figure 6: From left to right, we show how the ACR, AHR, TPR and JI metrics vary on the IDD experiment, by **varying the number of sentences selected for each cluster K** (top) and **varying the number of clusters C** (bottom). Note that $C = 1$ corresponds to not performing any clustering and, hence, analyzing the whole hard set *versus* the whole easy set. The very poor numbers obtained with $C = 1$ emphasizes the importance of clustering.

by using the entropy.

Finally, sentences referring to *fog* and *rain*, having scores slightly below the required condition ($\omega_{\theta}^{s_n} < \omega_{\theta}^{\text{avg}} - \beta$), are present in \mathcal{R}_S for all splitting strategies and most methods. One could interpret those as less severe false positives.

6.1.2 IDD

In the case of IDD, the best AHR/TPR/JI results in Fig. 2 are obtained with **SetDiff**. Yet, the lower ACR suggests that the sentences retained by this method have lower coverage in the cluster than the ones retained by the other methods. IDD is a large dataset with high content variation, hence, posing more challenges. Indeed, splitting into 15 clusters makes the content in each cluster

very heterogeneous (see Fig. 5) and therefore the selection of the three most *representative sentences* is rather difficult.

To tackle this complexity, we carry out two additional IDD experiments, varying *i*) the number of sentences selected and *ii*) the number of clusters.

Varying the number of retained sentences (K). We show in Fig. 6 (top) results for IDD as we vary the number of retained sentences per cluster. By increasing the number of sentences retained, we observe that the ACR increases for **FPDiff**, but decreases for the other methods; on the other hand, the ACR is stable starting from $K = 5$. The AHR is generally stable as we vary K , except for **FPDiff**, where we obtain the best value with $K = 1$. Both TPR and JI benefit from the increase of the number

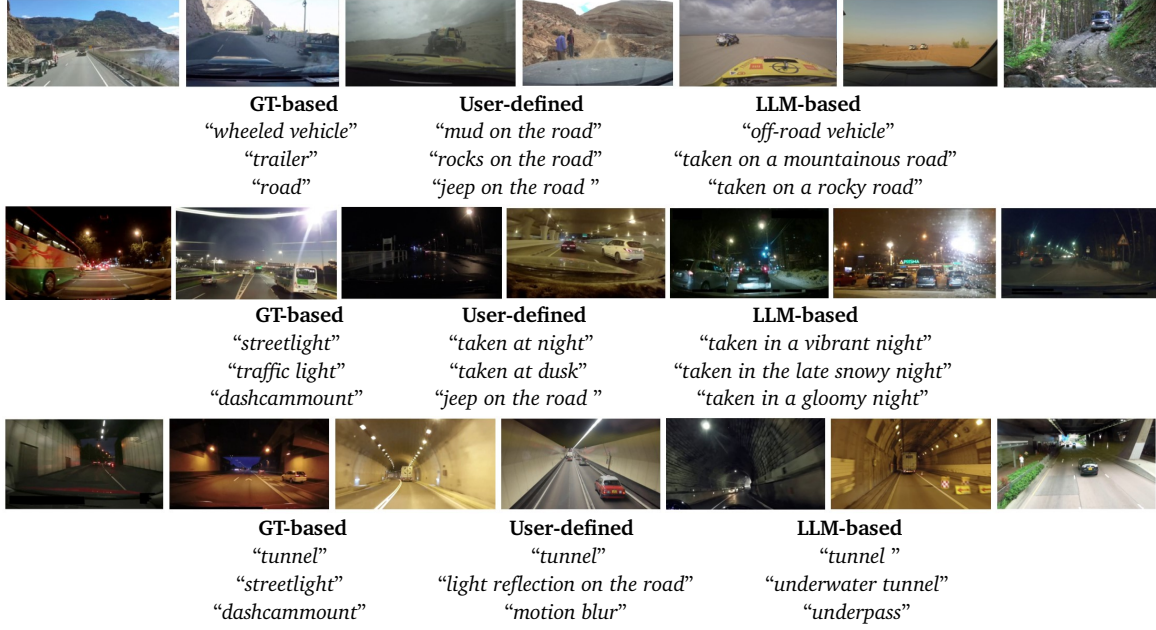


Figure 7: Three out of 15 hard clusters from WD2 (unsupervised case) explained by **FPDiff** when we use different the sentence sets (GT based, User defined or LLM generated).

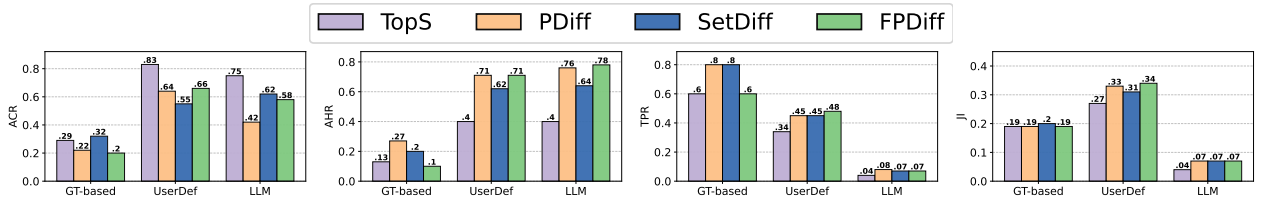


Figure 8: **Varying the sentence set.** Results obtained on WD2 when S is the GT-based, User-defined and the LLM-generated sentence set (see Appendix C.1).

of sentences (higher K). Overall, **SetDiff** outperforms the other methods in terms of AHR, TPR and JI. This result, combined with the low ACR, suggests that **SetDiff** is more capable of detecting rarer failure reasons, for which there are less support example images in the cluster/dataset.

Varying the number of clusters (C). In Fig. 6 (bottom) we present results obtained on IDD when we vary the number of clusters ($|C^h| = |C^e| = C$). By increasing the number of clusters, we observe an increase of the TPR (as expected) for all methods—with **PDiff** being the one that benefits the most. Concerning the other metrics, the default value $C = 15$ is a reasonable trade off. These experiments suggest that IDD is overall a very challenging set, with some of the failure causes under-represented—especially the ones related to the weather conditions (see sentences in Tab. 1 and Tab. 5), or not clustered together according to these characteristics (cf. Fig. 5). Furthermore, note that as the filtering in **FPDiff** relies on the **TopS** ranking, the very poor

performance of the latter on this particular set (IDD) affects negatively the performance of the former, making **PDiff** perform better than **FPDiff** when we consider more clusters or retain more sentences. Finally, the low performance obtained with $C = 1$ —corresponding to running the methods without the clustering step—shows that describing the full hard set by contrasting with the full easy set is a sub-optimal solution.

6.1.3 WD2

We analyse the performance of the different methods on WD2, varying the sentence set S . Indeed, for this dataset we have both User-defined (the same used throughout the experimental validation), a GT-based sentence sets, as well as a significantly larger LLM-based sentence set (see Appendix C). We show qualitative comparison in Fig. 7 and numerical results in Fig. 8.

Sensitivity to the choice of the sentence set. First, we notice that both the User-defined and



Figure 9: Three out of 15 hard clusters from NICO_{++}^{85} (unsupervised case) explained by different methods.

the LLM-generated sentence sets yield similar ACR and AHR scores. Yet, for the latter we have many sentences that are semantically related and carry similar hardness scores, for example “taken at night”/“mesmerizing moonlight”/“spellbound starlight”/“enigmatic night”/“miraculous midnight”. Since we limit the number of sentences each method can retrieve, in this case we cannot retrieve all of them with a small K and, in turn, this will result into significantly lower TPR and JI scores.

When we use the GT-based sentence set with $\alpha = 0.2$, \mathcal{S}_{β}^* contains only five sentences that are “showing a tunnel”, “showing a bridge”, “showing traffic light”, “showing a bus” and “showing snow”. Here, all methods introduce many false positives (explaining the low JI score). **PDiff** and **SetDiff** are able to retain four out of five sentences (except “showing a bus”) and **TopS** and **FPDiff** three out of five (missing also “showing a bridge”). The missing sentences had not enough image coverage in the clusters. The AHR and ACR scores are also low, due to the fact that it is not easy to find shared content for all clusters (see the low ACR even for **TopS**). Finally, note that the GT-based sentence set mainly describes the presence of the classes (“Image showing <class>”), therefore, it is not sufficient to describe the hard clusters to the desired level of details. This highlights the importance of properly designing \mathcal{S} , as well as the importance of using additional textual metadata to analyze the performance of our models.

6.1.4 NICO_{++}^{85}

We provide in Fig. 9 qualitative examples for NICO_{++}^{85} , in the unsupervised case (where we use the prediction entropy to split the data). We observe that our methods can capture the *context-class* associations that were rarely seen in the training set⁴ and hence the model struggles with their classification. Indeed we find “birds” or “plants” in “water” (top row), “landways” in the “rocks” (middle row) and “landways” in “dim lightning” (bottom row).

Next, we provide a sensitivity study on this dataset when we vary the hardness threshold value β .

Varying β (by varying α). Recall that β is the hyperparameter used to select the ground-truth sentence set \mathcal{S}^* , where higher β values imply retaining only the sentences with higher hardness scores as valid failure descriptions, while lower values imply that also sentences with a less strict hardness score are also considered as valid explanations. In Fig. 10 we show the impact of varying β on the AHR, TPR, and JI metrics. We carried out this experiment on the spurious classification task with NICO_{++}^{85} , considering the unsupervised case where we have GT image-sentence relevance scores (top row). As the number of sentences retained by the method is fixed ($K = 3$), varying β only affects \mathcal{S}^* and not $\mathcal{R}_{\mathcal{S}}$. Therefore, the value of ACR (that does not depend on

⁴See in Tab. 2 the distribution of the images in the validation set over the different classes-context pairs. Note that the validation set follows the training distribution.

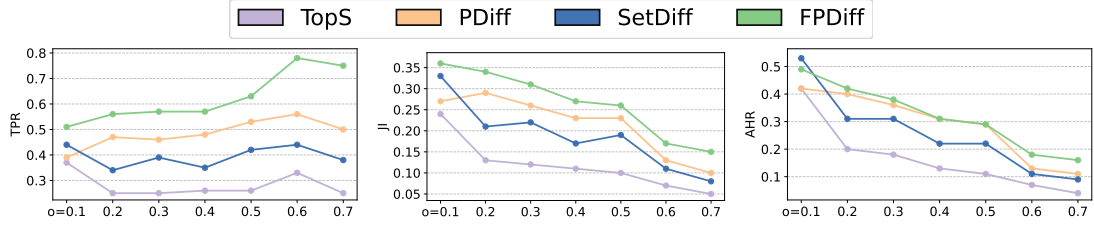


Figure 10: **Varying β (by varying o).** Results obtained on NICO₊₊⁸⁵ (unsupervised). The value β defines the ground truth set S^* , so its value impacts only the AHR/TPR/JI metrics (not the output of the methods or ACR). On x-axis: we plot o , where $\beta = o \cdot \omega_{\theta}^{\text{std}}$ with $\omega_{\theta}^{\text{std}}$ being the standard deviation of ω_{θ} (entropy) computed over \mathcal{X} .



Figure 11: Analyzing EfficientNet performance on the ImageNet 1K. The first two rows are from the "acoustic guitar" class, and the third is from the "bath tube" class.

β) is the same for each o value. Intuitively, with this study we assess how much each method focuses on the hardest sentences. Indeed, increasing the value of o (and hence increasing β) corresponds to accepting fewer and fewer sentences as valid explanations, namely the ones with the highest hardness score (lowest average accuracy). We observe that the **FPDiff** method, while experiencing a drop in performance as we make the problem harder, holds a better performance than the others methods for all the values of o .

6.1.5 ImageNet 1K

Finally, we focus on ImageNet 1K, where we treat each class separately. We can make several observations. *i*) When the error slices (hard clusters) mainly contain false positives from semantically similar classes or false

negatives with shared content, **TopS** will generally capture the shared characteristics—see examples in Fig. 11 (top two rows), Fig. 12 and Fig. 13 in Appendix E. *ii*) In the case of false positives with semantically similar classes, e.g., "electric guitar" and "banjo" in place of the "acoustic guitar" class (see first row in Fig. 11), the main difficulty for the other methods is that the same sentences are also highly ranked for the easy clusters, making it difficult for them to correctly identify the desired explanations—namely, contrasting the explanation between the easy and the hard clusters. This limitation is inherited from CLIP, which has difficulties to distinguish fine-grain classes. *iii*) When the false negatives share some semantic similarities and there is a candidate sentence that well describes this, all methods are able to find it. For example, see in Fig. 11 (second

row) the difficulty of the model to label the “*acoustic guitar*” when the photo is showing the person holding the guitar on a “*stage*”. Note that for these images **PDiff** and **FPDiff** also identified the “*blur*” as potential challenge (or “*low contrast*” and “*dim weather*” condition, in Fig. 12). iv) Finally, we have clusters where even for a human is difficult to describe what is common in the images beyond the object class. When there is a mix between false positives and false negatives, all methods including **TopS** have difficulties to identify the failure reason. In these cases, the selected sentences are relevant to some of the images in the cluster but they do not point to the reason for the failure (see Fig. 11 last row).

7. Concluding remarks

Assessing model performance, and in particular failure modes, for arbitrary task in arbitrary environments should be *easy*, *efficient* and *interpretable*. While the gold standard for performance evaluation is using a human-annotated test set, this process is costly and cannot scale for computer vision models to be deployed in many and diverse scenarios. Moreover, quantitative evaluation measures such as dataset-level accuracy values do not fully reflect the details of the model performance. It is important to know what lies beyond performance values and if the model is failing on particularly critical images.

In this work, we posit that it is of the utmost importance being able to assess model performance on non-annotated samples, and to move beyond hard-to-interpret numbers. We address this by first formulating the LBEE problem and designing a family of *task-agnostic* approaches that do not require error specifications or user-provided annotations. We complement these two contributions with different metrics to benchmark methods for LBEE and rely on those to carry out in-depth analyses. We show that we can retrieve relevant sentences pointing to important errors, e.g., related to environments beyond our model’s comfort zone.

In the future, we plan to overcome the need to define the sentence set S a priori. Indeed, while this design choice makes the evaluation more tractable and allows deploying our methods off the shelf, the set might omit certain unexpected failure reasons. A possible solution could be to build the sentence set S directly from the target set X , e.g., by running a captioner to describe all its images and merge these descriptions into the sentence set. Yet, in addition to being prohibitively expensive, a solution like this needs to be iterated for every new target set before running any method. Furthermore, in the case of a large image set, it would

also require further steps to remove redundancy and to regroup similar sentences.

References

- [1] Stanislaw Antol, Aishwarya Agrawal, Jiasen Lu, Margaret Mitchell, Dhruv Batra, Lawrence C. Zitnick, and Devi Parikh. VQA: Visual Question Answering. In *ICCV*, 2015. 19
- [2] Maximilian Augustin, Valentyn Boreiko, Francesco Croce, and Matthias Hein. Diffusion Visual Counterfactual Explanations. In *NeurIPS*, 2022. 3
- [3] Marius Cordts, Mohamed Omran, Sebastian Ramos, Timo Rehfeld, Markus Enzweiler, Rodrigo Benenson, Uwe Franke, Stefan Roth, and Bernt Schiele. The Cityscapes Dataset for Semantic Urban Scene Understanding. In *CVPR*, 2016. 5, 15
- [4] Pau de Jorge, Riccardo Volpi, Philip Torr, and Rogez Gregory. Reliability in Semantic Segmentation: Are We on the Right Track? In *CVPR*, 2023. 7
- [5] Greg d’Eon, Jason d’Eon, James R. Wright, and Kevin Leyton-Brown. The Spotlight: A General Method for Discovering Systematic Errors in Deep Learning Models. In *ACM FAccT*, 2022. 2
- [6] Finale Doshi-Velez and Been Kim. Towards A Rigorous Science of Interpretable Machine Learning. arXiv:1702.08608, 2017. 1
- [7] Alexey Dosovitskiy, Lucas Beyer, Alexander Kolesnikov, Dirk Weissenborn, Xiaohua Zhai, Thomas Unterthiner, Mostafa Dehghani, Matthias Minderer, Georg Heigold, Sylvain Gelly, Jakob Uszkoreit, and Neil Houlsby. An Image is Worth 16x16 Words: Transformers for Image Recognition at Scale. In *ICLR*, 2021. 16
- [8] Lisa Dunlap, Yuhui Zhang, Xiaohan Wang, Ruiqi Zhong, Trevor Darrell, Jacob Steinhardt, Joseph E. Gonzalez, and Serena Yeung-Levy. Describing Differences in Image Sets with Natural Language. In *CVPR*, 2024. 2
- [9] Sabri Eyuboglu, Maya Varma, Khaled Saab, Jean-Benoit Delbrouck, Christopher Lee-Messer, Jared Dunnmon, James Zou, and Christopher Ré. Domino: Discovering Systematic Errors with Cross-Modal Embeddings. In *ICLR*, 2022. 1, 2, 3, 5, 6, 16, 17, 18
- [10] Irena Gao, Gabriel Ilharco, Scott Lundberg, and Marco Tulio Ribeiro. Adaptive Testing of Computer Vision Models. In *ICCV*, 2023. 2
- [11] Yash Goyal, Ziyang Wu, Jan Ernst, Dhruv Batra, Devi Parikh, and Stefan Lee. Counterfactual Visual Explanations. In *ICML*, 2019. 3
- [12] Kaiming He, Xiangyu Zhang, Shaoqing Ren, and Jian Sun. Deep Residual Learning for Image Recognition. In *CVPR*, 2016. 16
- [13] Lisa Anne Hendricks, Zeynep Akata, Marcus Rohrbach, Jeff Donahue, Bernt Schiele, and Trevor Darrell. Generating Visual Explanations. In *ECCV*, 2016. 3
- [14] Lisa Anne Hendricks, Kaylee Burns, Kate Saenko, Trevor Darrell, and Anna Rohrbach. Women also Snowboard: Overcoming Bias in Captioning Models. In *ECCV*, 2018. 6

- [15] Lisa Anne Hendricks, Ronghang Hu, Trevor Darrell, and Zeynep Akata. Grounding Visual Explanations. In *ECCV*, 2018. 3
- [16] Lisa Anne Hendricks, Ronghang Hu, Trevor Darrell, and Zeynep Akata. Generating Counterfactual Explanations with Natural Language. In *ICML Workshops*, 2018. 3
- [17] Gabriel Ilharco, Mitchell Wortsman, Ross Wightman, Cade Gordon, Nicholas Carlini, Rohan Taori, Achal Dave, Vaishaal Shankar, Hongseok Namkoong, John Miller, Hannaneh Hajishirzi, Ali Farhadi, and Ludwig Schmidt. OpenCLIP. Zenodo, https://github.com/mlfoundations/open_clip, 2021. 3, 6, 20
- [18] Paul Jacob, Éloi Zabolocki, Hédi Ben-Younes, Mickaël Chen, Patrick Pérez, and Matthieu Cord. STEEX: Steering Counterfactual Explanations with Semantics. In *ECCV*, 2022. 3
- [19] Saachi Jain, Hadi Salman, Eric Wong, Pengchuan Zhang, Vibhav Vineet, Sai Vemprala, and Aleksander Madry. Missingness Bias in Model Debugging. In *ICLR*, 2022. 2
- [20] Saachi Jain, Hannah Lawrence, Ankur Moitra, and Aleksander Madry. Distilling Model Failures as Directions in Latent Space. In *ICLR*, 2023. 1, 2, 3
- [21] Guillaume Jeanneret, Loïc Simon, and Frédéric Jurie. Diffusion Models for Counterfactual Explanations. In *ACCV*, 2022. 3
- [22] Jinkyu Kim, Anna Rohrbach, Trevor Darrell, John Canny, and Zeynep Akata. Textual Explanations for Self-Driving Vehicles. In *ECCV*, 2018. 3
- [23] Younghyun Kim, Sangwoo Mo, Minkyu Kim, Kyungmin Lee, Jaeho Lee, and Jinwoo Shin. Discovering and Mitigating Visual Biases through Keyword Explanation. In *CVPR*, 2024. 2
- [24] Junnan Li, Dongxu Li, Caiming Xiong, and Steven Hoi. BLIP: Bootstrapping Language-Image Pre-training for Unified Vision-Language Understanding and Generation. In *ICML*, 2022. 20
- [25] Weixin Liang, Yuhui Zhang, Yongchan Kwon, Serena Yeung, and James Zou. Mind the Gap: Understanding the Modality Gap in Multi-modal Contrastive Representation Learning. In *NeurIPS*, 2022. 4
- [26] Evan Z Liu, Behzad Haghighi, Annie S Chen, Aditi Raghunathan, Pang Wei Koh, Shiori Sagawa, Percy Liang, and Chelsea Finn. Just Train Twice: Improving Group Robustness without Training Group Information. In *ICML*, 2021. 2
- [27] Haotian Liu, Chunyuan Li, Qingyang Wu, and Yong Jae Lee. Visual Instruction Tuning. In *NeurIPS*, 2023. 20
- [28] Ziwei Liu, Ping Luo, Xiaogang Wang, and Xiaoou Tang. Deep Learning Face Attributes in the Wild. In *ICCV*, 2015. 2
- [29] Zhuang Liu, Hanzi Mao, Chao-Yuan Wu, Christoph Feichtenhofer, Trevor Darrell, and Saining Xie. A ConvNet for the 2020s. In *CVPR*, 2022. 5, 15
- [30] Jan Hendrik Metzen, Robin Huttmacher, N. Grace Hua, Valentyn Boreiko, and Dan Zhang. Identification of Systematic Errors of Image Classifiers on Rare Subgroups. In *ICCV*, 2023. 2
- [31] Ron Mokady, Amir Hertz, and Amit H. Bermano. ClipCap: CLIP Prefix for Image Captioning. arXiv:2111.09734, 2021. 5
- [32] Alec Radford, Jong Wook Kim, Chris Hallacy, Aditya Ramesh, Gabriel Goh, Sandhini Agarwal, Amanda Sastry, Girishan Askell, Pamela Mishkin, Jack Clark, Gretchen Krueger, and Ilya Sutskever. Learning Transferable Visual Models From Natural Language Supervision. In *ICML*, 2021. 2
- [33] Pengzhen Ren, Yun Xiao, Xiaojun Chang, Po-Yao Huang, Zhihui Li, Brij B Gupta, Xiaojang Chen, and Xin Wang. A survey of deep active learning. *ACM computing surveys (CSUR)*, 54(9):1–40, 2021. 7
- [34] Keivan Rezaei, Mehrdad Saberi, Mazda Moayeri, and Soheil Feizi. PRIME: Prioritizing Interpretability in Failure Mode Extraction. In *ICLR*, 2024. 1, 2
- [35] Marco Tulio Ribeiro, Sameer Singh, and Carlos Guestrin. ‘Why Should I Trust You?’ Explaining the Predictions of any Classifier. In *SIGKDD*, 2016. 3
- [36] Olga Russakovsky, Jia Deng, Hao Su, Jonathan Krause, Sanjeev Satheesh, Sean Ma, Zhiheng Huang, Andrej Karpathy, Aditya Khosla, Michael S. Bernstein, Alexander C. Berg, and Li Fei-Fei. ImageNet Large Scale Visual Recognition Challenge. *International Journal of Computer Vision (IJCV)*, 115:211–252, 2015. 16, 19
- [37] Christos Sakaridis, Dengxin Dai, and Luc Van Gool. ACDC: The Adverse Conditions Dataset with Correspondences for Semantic Driving Scene Understanding. In *ICCV*, 2021. 5, 15
- [38] Fawaz Sammani, Tanmoy Mukherjee, and Nikos Deligiannis. NLX-GPT: A Model for Natural Language Explanations in Vision and Vision-Language Tasks. In *CVPR*, 2022. 3
- [39] Christoph Schuhmann, Romain Beaumont, Richard Vencu, Cade Gordon, Ross Wightman, Mehdi Cherti, Theo Coombes, Aarush Katta, Clayton Mullis, Mitchell Wortsman, Patrick Schramowski, Srivatsa Kundurthy, Katherine Crowson, Ludwig Schmidt, Robert Kaczmarczyk, and Jenia Jitsev. LAION-5B: An Open Large-scale Dataset for Training Next Generation Image-text Models. In *NeurIPS*, 2022. 20
- [40] Ramprasaath R. Selvaraju, Michael Cogswell, Abhishek Das, Ramakrishna Vedantam, Devi Parikh, and Dhruv Batra. Grad-CAM: Visual Explanations from Deep Networks via Gradient-based Localization. In *ICCV*, 2017. 3
- [41] Burr Settles. Active learning literature survey. *Technical Report. University of Wisconsin-Madison Department of Computer Sciences*, 2009. 7
- [42] Sahil Singla, Besmira Nushi, Shital Shah, Ece Kamar, and Eric Horvitz. Understanding Failures of Deep Networks via Robust Feature Extraction. In *CVPR*, 2021. 2
- [43] Mingxing Tan and Quoc V. Le. EfficientNet: Rethinking Model Scaling for Convolutional Neural Networks. In *ICML*, 2019. 16
- [44] Osman Tursun, Simon Denma, Sridha Sridharan, and Clinton Fookes. Towards Self-Explainability of Deep

Neural Networks with Heatmap Captioning and Large-Language Models. arXiv:2304.02202, 2023. 3

- [45] Girish Varma, Anbumani Subramanian, Anoop Nambodiri, Manmohan Chandraker, and C.V. Jawahar. IDD: A Dataset for Exploring Problems of Autonomous Navigation in Unconstrained Environments. In *WACV*, 2019. 5, 15
- [46] Joshua Vendrow, Saachi Jain, Logan Engstrom, and Aleksander Madry. Dataset Interfaces: Diagnosing Model Failures Using Controllable Counterfactual Generation. In *ICML Workshops*, 2024. 3
- [47] Peng Wang, An Yang, Rui Men, Junyang Lin, Shuai Bai, Zhikang Li, Jianxin Ma, Chang Zhou, Jingren Zhou, and Hongxia Yang. OFA: Unifying Architectures, Tasks, and Modalities Through a Simple Sequence-to-Sequence Learning Framework. In *ICML*, 2022. 20
- [48] Joe H. Ward. Hierarchical Grouping to Optimize an Objective Function. *Journal of the American Statistical Association*, 58(301):236—244, 1963. 4
- [49] Olivia Wiles, Isabela Albuquerque, and Sven Gowal. Discovering Bugs in Vision Models using Off-the-shelf Image Generation and Captioning. In *NeurIPS*, 2022. 1, 2
- [50] Eric Wong, Shibani Santurkar, and Aleksander Madry. Leveraging Sparse Linear Layers for Debuggable Deep Networks. In *ICML*, 2021. 2
- [51] Sriram Yenamandra, Pratik Ramesh, Viraj Prabhu, and Judy Hoffman. FACTS: First Amplify Correlations and then Slice to Discover Bias. In *ICCV*, 2023. 1, 2, 3, 5, 6, 15, 16, 17, 18
- [52] Oliver Zendel, Katrin Honauer, Markus Murschitz, Daniel Steininger, and Gustavo Fernandez Dominguez. WildDash - Creating Hazard-Aware Benchmarks. In *ECCV*, 2018. 5, 15, 18, 20
- [53] Jianming Zhang, Sarah Adel Bargal, Zhe Lin, Jonathan Brandt, Xiaohui Shen, and Stan Sclaroff. Top-down Neural Attention by Excitation Backprop. In *ECCV*, 2018. 3
- [54] Xingxuan Zhang, Yue He, Renzhe Xu, Han Yu, Zheyang Shen, and Peng Cui. NICO++: Towards Better Benchmarking for Domain Generalization. In *CVPR*, 2023. 15
- [55] Jieyu Zhao, Tianlu Wang, Mark Yatskar, Vicente Ordonez, and Kai-Wei Chang. Men Also Like Shopping: Reducing Gender Bias Amplification using Corpus-level Constraints. In *EMNLP*, 2017. 6
- [56] Bolei Zhou, Agata Lapedriza, Aditya Khosla, Aude Oliva, and Antonio Torralba. Places: A 10 million Image Database for Scene Recognition. *IEEE Transactions on Pattern Analysis and Machine Intelligence (PAMI)*, 40(6): 1452–1464, 2018. 16, 19

Appendix

A. Datasets and Tasks

In the following, we detail the three main tasks we tackle in this paper: semantic segmentation of urban scenes, classification in the presence of spuriously correlated data, and ImageNet-1K classification.

Urban scene segmentation. We consider a ConvNeXt [29] segmentation model trained on Cityscapes [3], comprised of images from 50 European cities collected at daytime in clear weather conditions. We build our evaluation sets \mathcal{X} using three datasets: *i*) WildDash 2 (WD2) [52], which contains challenging visual conditions such as motion blur, various road types, difficult weather, *etc.* and *ii*) India Driving Dataset (IDD) [45], which contains images from Hyderabad, Bangalore and their peripheries, *iii*) ACDC [37] contains images recorded in adverse conditions, namely *fog*, *rain*, *snow* and *night* representing challenging domain shift for the Cityscapes model. For the main experiments we use the user-defined sentence set \mathcal{S} with 148 sentences describing content related to urban scenes, road conditions, and image quality (described in Appendix C). In Sec. 6.1.3 we compare these results with the results obtained on WD2 when using both a smaller GT-based sentence set derived from the metadata information available with the dataset and a larger sentence set of 1016 sentences generated automatically by an LLM (both sets detailed in Appendix C).

Classification with spurious correlations. We use the NICO++ [54] dataset, consisting of real-world images of concept classes (*mammals*, *birds*, *plants*, *airways*, *landways* and *waterways*) taken in six contexts (*dim lighting*, *outdoor*, *grass*, *rock*, *autumn*, *water*). We follow the train, biased validation, and unbiased test splits from [51], aimed at creating different levels of class-context correlations. We use three partitionings NICO₊₊⁷⁵, NICO₊₊⁸⁵ and NICO₊₊⁹⁵ with increased levels of correlation.⁵ We train a ResNet-50 model on each training set, and use the unbiased test set for evaluation.

To evaluate error descriptions of the hard clusters, we build a sentence set \mathcal{S} with 130 sentences that include information related to the the six classes, the six contexts, various sub-classes and their combination. Note that in this case we have GT relevance $\Gamma(\mathbf{x}_m, s_n)$ between sentences and images.

We consider two cases, an unsupervised and a supervised one. In the former case, we consider the full

⁵This means setting the correlation level to 75%, 85% and 95% respectively between a class and its natural context in the training/validation set, as detailed in [51].

set and split it with entropy values computed on class predictions. In the latter case, similarly to [9, 51], we consider images from each class separately and use the class probability scores to split the data into easy and hard sets.

ImageNet-1K classification. We consider three different architectures (ResNet-50 [12], ViT-B-16 [7], and EfficientNet-B1 [43]) trained on the ImageNet-1K [36] training set and evaluate these models on the ImageNet-1K validation set. We build S as the union of a set of sentences $\{\text{"An image of a <class>"}\}$ (for the 1K classes) with a set of sentences corresponding to some place classes from Places365 [56] in form of $\{\text{"An image taken at <location>"}\}$, and a set of sentences describing image type (photo, drawing), image quality (blurry, noise, JPEG compression), weather conditions, *etc.* In total we have 1417 sentences (see details in Appendix C). To assess the relevance between a sentence and an image, we use a combination of ground truth based information (for the first 1000 sentences corresponding to the 1000 class names) and a VQA model to assess the relevance for the other sentences (as described in Appendix C.3).

With this dataset, we focus on the top-1 classification performance of different models and aim at analyzing failure cases for this task—namely, the reasons for not predicting the correct class on top. In ImageNet classification, several errors arise from confusions between semantically similar classes. For example, the model will miss-classify dog breeds, bird/fish species, similar objects, *etc.* In such cases, knowing the correct class label can help to deduce the main reason from the retrieved description. Indeed, for example, if the selected sentence is $\{\text{"An image of a water snake"}\}$ without the knowledge of the correct class, it is difficult to interpret whether the model predicts false positives (images of different type of snakes) or the model failed to recognize the water snake (false negative) for some reasons. Furthermore, while, class independent failure reasons such as those related to image capturing conditions (e.g. blurred or low contrast images) might emerge when processing the full dataset as a whole, errors related to the image content is more difficult to interpret if it is a failure reason without the knowledge of the target class (e.g. finding that the image was taken at a *beach* has different effect on the model for the *swimming suit* class than for the *cow* or *ski suit* class). Finally, even if we use a very large number of clusters with the full set, the content of the nearest easy cluster might differ in many aspects from the hard one, making rather it difficult to select in priority which is the one causing the model to fail.

For all these reasons we opted to follow the prior art and apply LBEE methods by analyzing the data for each class independently. Still, in contrast to prior art, where only false negative errors are considered (the images that belong to the given class but labeled with a wrong class label), we also include false positives. Hence, the easy set X^e contains the images where the class has been correctly predicted (images from the current class) while the hard set is a union of false positives and false negatives.

B. Comparison with prior art

DOMINO [9] and FACTS [51] mainly focus on evaluating the error mode discovery [9, 51], assuming to know the set of error types, and limit the language description of these error modes to a qualitative role. In contrast, in our problem formulation, we treat the language-based description of errors made by computer vision models as the problem itself. For this reason, a direct comparison with prior art is not straightforward. In this section, we make an attempt by simply comparing our split-and-cluster partitioning to the more complex, learnt partitioning methods by [9, 51], following their evaluation protocol.

We perform this analysis using the NICO₊₊⁷⁵, NICO₊₊⁸⁵ and NICO₊₊⁹⁵ sets from [51], corresponding to a 75%, 85% and 95% correlation level, respectively, between the classes and their natural context in the training set. This artificially introduces strong spurious correlations between classes and contexts, makes the model to fail in scenarios where the test set does not follow the same biased distribution seen at training.

To tackle this setting, [51] propose to learn a partitioning Gaussian Mixture model on a *Biased* validation set that follows the same bias as the training set and evaluate the partitioning on an *Unbiased* set where all class-context are equally represented (see statistics in Tab. 2). Note that this is done for each class independently (per-class case). Using the code provided by [51]⁶, we learn and evaluate all possible set combinations (see Tab. 3). Note that (*Biased-Biased*) and (*Unbiased-Unbiased*) sets means that we learnt and test the partitioning function on the exact same data.

In our case, there is no learning involved: we simply split and cluster the data as discussed in Sec. 4. Then, for a given (A, B) pair of sets, where $A, B \in \{\text{Biased, Unbiased}\}$, we assign images from the set B to the cluster prototypes obtained with the images in set A , where the union of easy and hard prototypes is considered. We use the class probability to split the

⁶<https://github.com/yvsriram/FACTS>

Table 2: The number of images in the *Biased* validation set for each (class, context) pair in corresponding three NICO++ datasets. The *Unbiased* validation sets have 50 images for each (class, context) pairs in each of the three sets. The spurious contexts (1 to 6) are in order *rock*, *grass*, *dim lighting*, *autumn*, *water*, *outdoor*.

NICO++ set class ↓ context →	NICO ⁹⁵ ₊₊						NICO ⁸⁵ ₊₊						NICO ⁷⁵ ₊₊					
	1	2	3	4	5	6	1	2	3	4	5	6	1	2	3	4	5	6
mammals	638	4	2	2	3	3	638	4	2	2	3	3	638	10	5	7	8	9
birds	7	321	2	2	3	3	7	321	2	2	3	3	19	321	5	7	8	9
plants	7	4	154	2	3	3	7	4	154	2	3	3	19	10	154	7	8	9
airways	7	4	2	220	3	3	7	4	2	220	3	3	19	10	5	220	8	9
waterways	7	4	2	2	266	3	7	4	2	2	266	3	19	10	5	7	266	9
landways	7	4	2	2	3	277	7	4	2	2	3	277	19	10	5	7	8	277

data—the same measure used by FACTS [51] to learn the partitioning function, except that we only use the probability of the target class while they use the probabilities of all classes.

Evaluation protocol. Before discussing the comparative results, we recall the metrics and the evaluation protocol we use, proposed by [9, 51]. In particular they propose to rely on the Precision-at-K ($P@K$) to measure how accurately a partitioning method aggregates samples from the same context given a class. Formally, let \mathcal{X} denote the test set, $\{\mathbf{z}_n\}_{n=1}^N$ the ground-truth partitions and $\{\hat{\mathbf{z}}_m\}_{m=1}^M$ the predicted set of discovered partitions. Given K , for each ground-truth partition \mathbf{z}_n the most "similar" predicted partition $\hat{\mathbf{z}}_m$ is selected based on the size of the intersection $\mathbf{z}_n \cap \hat{\mathbf{z}}_m^K$, where $\hat{\mathbf{z}}_m^K$ is the subset containing the top- K elements of \mathcal{X} according to the likelihood of belonging to $\hat{\mathbf{z}}_m$. For FACTS/DOMINO the ranking corresponds to the partitioning function's output, while in our case to the assignment to the closest prototype. If we denote by $\hat{\mathbf{z}}_{nm}^K$ the set that has the largest overlap with \mathbf{z}_n given K , the $P@K$ is defined as

$$P@K = \frac{1}{N} \sum_{n=1}^N \frac{|\mathbf{z}_n \cap \hat{\mathbf{z}}_{nm}^K|}{K}$$

where the average is computed, as in [51], over the five bias-conflicting groups (excluding the spuriously correlated GT partitions, such as the context *water* for *waterways*).

Experimental results. We show in Tab. 3 the $P@K$ values averaged over the six classes for the different NICO++ sets. Each time we show results averaged over three different variants of the current model trained with different seed⁷. In our case, we used the exact same ResNet50 models and the same *Biased* and

Unbiased sets on which we perform the split and the clustering. We use five easy and five hard clusters as it is our default setting for the per-class case and as in the code from [51] the default number of slices was also set to ten.

From Tab. 3 we can see that our split-and-cluster method provides competitive, or sometimes even better, slice discovery performance than the more complex partition learning methods. Our method performs slightly worse than FACTS on the *Unbiased* set both when their partitioning was trained on the *Unbiased* or on the *Biased* set. Surprisingly though, both FACTS and DOMINO underperform when tested on the *Biased* set even when the partitioning function was trained on this set. In contrast, our method is more robust and performs similarly on both sets. When the FACTS model is trained on the *Biased* set, which strongly relies on priors about class-context associations (the configuration shown in their paper), it outperforms our model, for which the $P@K$ decreases as the amount of class-context correlation increases (bottom part of Tab. 3). We hypothesize that the reason behind this result is that we do not have enough data for a proper clustering (see Tab. 2), while FACTS manages to learn the partitioning function even with a few samples by exploiting the strong correlation between the classes and dominant context. As the model is trained mainly with images with specific combinations of class and correlated context—for example, mammals in rocky environments—the model rarely sees images from other classes in this context. Consequently, when the model learns to predict a class "c" with high probability, it also associates this high probability with the presence of the corresponding context (e.g. rocks) even if the class (*mammals*) is absent. Therefore, when analyzing another class, such as *plants*, and learn the partitioning based on all six probabilities, the partitioning function primarily learns to assign images based on the highest probability score, which is an indicator of the context. For instance, a plant image taken in a rocky environment will have a high probability score for the mammal class, indicating the

⁷Since we were not able to reproduce the original paper's numbers with the code, namely, the results corresponding to the (*Biased*, *Unbiased*) pairs, for fairness we ran their code with three different seeds and provide here the averaged results. We do not show the variances in the table to keep it simple, but the values are most often between 1 and 2.

Table 3: **Comparisons with prior art.** We compare the clustering obtained via Step 3 of our proposed methods (see Fig. 1) with the Domino and FACTS using averaged $P@K$ scores with $K = 10$. For our method, we split the dataset into 5 “easy” and 5 “hard” clusters and use their union as final partitioning. On the top rows (below Random) we show results obtained with the partitioning learnt on the *Unbiased* set and on the bottom rows the results were obtained when the partitioning is learnt on the *Biased* set. Random corresponds to assigning the test data randomly to the partitions.

Method Test set →	NICO ₊₊ ⁷⁵		NICO ₊₊ ⁸⁵		NICO ₊₊ ⁹⁵	
	Unbiased	Biased	Unbiased	Biased	Unbiased	Biased
Random	29.7	12.6	32.0	14.0	33.0	14.6
Domino [9]	44.4	12.1	47.0	12.3	52.7	22.3
FACTS [51]	58.8	28.1	63.6	30.0	68.9	39.9
Ours(5-5)	53.6	52.3	54.2	58.4	55.3	66.1
Domino [9]	26.0	17.1	19.0	19.8	17.4	25.6
FACTS [51]	53.3	31.4	53.2	28.7	58.9	34.4
Ours(5-5)	51.3	52.2	46.8	52.5	41.9	46.5

presence of rocks. Note that in our case, when analyzing the plant class, we disregard the probabilities of other classes, thereby using much less prior information about the image context.

In summary, despite the simplicity of our method, it performs favorably to prior art in their proposed settings, while also being able to provide natural language descriptions of error modes as shown in Sec. 6.

C. Defining the sentence sets

Our paper focuses on two objectives, 1) identifying error modes in computer vision models and 2) describing them with natural language. To achieve this, we rely on a large set of sentences (S), that can either be provided or automatically generated. This sentence set is expected to cover various potential reasons for model failures given a task. In this section, we first discuss three approaches to construct such sentence sets (Appendix C.1); then we detail how we create the ground-truth sentence set S_{β}^* for LBEE (Appendix C.2); finally, we show how to obtain pseudo-GT relevance scores between images and sentences using Visual-Question Answering (VQA) tools when not available otherwise (Appendix C.3).

C.1. Building the sentence set S

There are several possibilities to construct the sentence sets S . We describe a few possibilities below.

User-defined. The set of sentences can be designed ad hoc for the task at hand by the end user who has the expert knowledge and can envisage the main difficulties a model might face. While such sentence set might be non-exhaustive, it can cover the most important

failure causes. Our method aim to select from them the ones that confirm the user’s concerns (with additional visual support). In this case, to get pseudo-ground-truth relevance between images and a sentence, we resort to VQA (as described in Appendix C.3).

We follow this setting to build S in our experiments on the urban scene segmentation task. More specifically, we manually defined 148 sentences describing content related to urban scenes (buildings, pedestrians, traffic, two-wheels, trees, animals, garbage, *etc.*) in the form of {“An image of a <urban scene content>”}, road conditions (weather, lighting, season) in form of {“An image taken in/at <condition>”} or image quality (underexposure, motion blur, *etc.*) in form of {“An image with <effect>”}. A large subset of this sentence set can be seen in Tab. 5.

GT-based. If available, we can use ground-truth information (class labels and metadata) to generate a sentence set. This is quite limiting in general: we mainly use this option because it yields the advantage of providing the GT relevance between images and sentences. We used this option in all NICO++ experiments, where we build 130 sentences that include combinations from the six classes, the six contexts, and various sub-class information. For example, we have {“A photo of <sub-class> in the <context>”} such as “A photo of a cactus in the water”.

We also built a GT-based sentence set for the WD2 dataset [52] tested in the context of urban scene segmentation task. It contains annotations for 81 classes, from which we selected 74 classes (removing the ambiguous ones most difficult for VLMs to handle, namely ‘unlabeled’, ‘ego-vehicle’, ‘overlay’, ‘out-of-roi’, ‘static’, ‘dy-

namic, ‘*curb terrain*’). The sentences have the form {“*An image showing a <class>*”}, where *<class>* was replaced each time by one of the 74 classes selected. While this allows us to generate GT relevance scores for each image in WD2, this set limits our methods in selecting only from failure causes related to the presence of these classes in the image and hence they do not cover all the possible failure reasons that may explain the model’s behavior.

In the case of ImageNet-1K [36], the first 1K sentences (out of 1417) were also generated from the GT information, namely the class names. We consider sentences with the form {“*An image of a <class>*”}. This was complemented by a set of user-defined sentence set related to various places in the form {“*An image taken in <location>*”} where we filled the *<location>* with the place class names from Places365 [56]. Finally we also added a set of sentences describing image type (photo, drawing), image quality (blurry, noise, JPEG compression), weather conditions, *etc.* yielding to a total of 1417 sentence set used for ImageNet-1K.

LLM-generated. In the case of urban scene segmentation task, we also consider a set of sentences generated by a large language model (LLM). We provided GPT-3.5 with the context and the sentence structure and prompted it to provide lists of sentences related to weather conditions, vehicles, urban objects, time of day and road conditions. For each of them we used either the sentence form {“*An image taken in/at <weather/road condition or time of day>*”} or {“*An image showing a/an <vehicle/urban object>*”}, where the template is filled by the LLM. This yields to a set of 1016 sentences, including most of the ones we design manually in the User-defined set. On the other end, the limitation of this approach is the noise in the set, which can also include sentences hardly helpful for the task at end, *e.g.* “*An image taken on an unpredictable/eclectic/dystopian road*” or “*An image taken in a corn maze/trick-or-treat/pajama weather*”.

C.2. Defining the ground-truth S_β^* for LBEE

To evaluate the predicted sentence set $\mathcal{R}_S \subset \mathcal{S}$ output by an LBEE approach, we must define a set of ground-truth sentences $S^* \subset \mathcal{S}$ to compare our predictions to—namely, ground-truth error mode descriptions. To derive such GT set, we consider the function $\omega_\theta : \mathbb{R}^{H \times W \times 3} \rightarrow \mathbb{R}$ that measures the model’s performance on each image \mathbf{x}_i . This function can be the accuracy in the case of a classification task, the mIoU (mean Intersection over Union) score for semantic segmentation, or any other task-specific metric. Given the

set of images \mathcal{X} , the average value of this measure over the entire dataset

$$\omega_\theta^{\text{avg}} = \frac{1}{|\mathcal{X}|} \sum_{\mathbf{x}_m \in \mathcal{X}} \omega_\theta(\mathbf{x}_m) , \quad (6)$$

is the overall performance of \mathcal{M}_θ on \mathcal{X} .

Given this value and a threshold β , we define the ground-truth sentence set S^* , associated with failure cases of \mathcal{M}_θ on \mathcal{X} , as the set of sentences for which the mean performance across images associated with the sentence falls beneath the overall mean performance by a given margin β . To retrieve the images associated with a sentence, we define a binary function $\Gamma(\mathbf{x}_m, s_n)$ that outputs 1 if the sentence s_n describes the image \mathbf{x}_m (*i.e.*, is relevant to it), and 0 otherwise. For example, if \mathbf{x}_m is an image taken at night, $\Gamma(\mathbf{x}_m, \text{“Image taken at night”}) = 1$ whereas $\Gamma(\mathbf{x}_m, \text{“Image taken at sunset”}) = 0$. If this relevance cannot be derived directly from ground truth information (most of the cases), we resort to VQA [1] to obtain such information for arbitrary sentences on arbitrary datasets—as detailed in Appendix C.3.

The set of images associated with a sentence s_n is defined as

$$\mathcal{X}_{s_n} = \{\mathbf{x}_m \in \mathcal{X} | \Gamma(\mathbf{x}_m, s_n) = 1\} . \quad (7)$$

Then, for each sentence we compute a score by averaging the model performance over the associated images

$$\omega_\theta^{s_n} = \frac{1}{|\mathcal{X}_{s_n}|} \sum_{\mathbf{x}_m \in \mathcal{X}_{s_n}} \omega_\theta(\mathbf{x}_m) . \quad (8)$$

We use this quantity to represent the sentence’s *hardness* score (according to the measure ω_θ) and we consider a sentence as *describing a failure mode* if its value is below the global average $\omega_\theta^{\text{avg}}$ by at least a margin β . Therefore, the desired output S^* is the collection of all of these sentences:

$$S^* = \{s_n \in \mathcal{S} | \omega_\theta^{s_n} < \omega_\theta^{\text{avg}} - \beta\} . \quad (9)$$

Varying β allows to evaluate the methods with different severity levels for the desired error descriptions, *i.e.*, a higher β restricts the desired set S^* to more challenging sentences (see Fig. 10).

C.3. Pseudo-GT image-sentence relevance

When we do not have access to GT information, we rely on VQA [1] to determine whether an image $\mathbf{x}_m \in \mathcal{X}$ can be associated with a sentence s_n (description) or not. These binary relevance scores $\Gamma(\mathbf{x}_m, s_n)$ are necessary to define the GT sentence set S^* for LBEE (see Appendix C.2) but also to derive the sentence coverage ratio in the cluster (CR defined in Sec. 5).

Table 4: Comparison of pseudo-ground truth annotations created using LLaVA and OFA with manual ground truth annotations in WD2.

Model	Accuracy↑	TP↑	TN↑	FP↓	FN↓
OFA	0.799	0.489	0.852	0.148	0.511
LLaVA	0.731	0.623	0.696	0.304	0.377
OFA LLaVA	0.701	0.735	0.642	0.358	0.265
OFA & LLaVA	0.829	0.377	0.905	0.095	0.623

In particular, we use OFA [47] and LLaVA [27] with their publicly available pre-trained weights—but any other (possibly more recent) model can be used instead. We do not simply use OFA and LLaVA alone, but we also combine them: combining the CLIP-based LLaVA with non CLIP-based OFA representation allow us to significantly decrease the CLIP bias from the pseudo-GT relevance scores.

To proceed with VQA, we first turn each sentence $s_n \in \mathcal{S}$ into a question q_n such that the expected answer is *yes* or *no*. For example the sentence “An image taken at night” was turned into the prompt: “Was the image taken at night? Reply simply with ‘yes’ or ‘no’.”. Then we provide VQA model with the image-question pairs (x_i, q_n) and turn the yes/no answer into a binary score that is assigned to $\Gamma(x_i, s_n)$.

Comparing VQA pseudo-GT to manually annotated GT. Given the key role that VQA plays in our experimental validation, we carry out an experimental analysis to compare the pseudo-GT image-sentence associations obtained with LLaVA [27] and/or OFA [47] to manually annotated GT. To this end, we rely on the GT annotations from WD2 [52] and the derived 74 sentences (described in Appendix C.1) from which we compute the GT scores for $\Gamma(x_i, s_n)$. Turning these sentences into questions, we can gather the pseudo-GT relevance scores $\Gamma_{\text{OFA}}(x_i, s_n)$ and $\Gamma_{\text{LLaVA}}(x_i, s_n)$.

We evaluate the accuracy of these pseudo-GT associations independently, as well as combined with AND/OR logical operations (**OFA & LLaVA** and **OFA | LLaVA**, respectively) and report our results in Tab. 4. Combining the output from both models yields the highest accuracy with respect to the ground-truth. Moreover, the accuracy of both models achieves an accuracy above 70% of the GT performance, with **LLaVA** hallucinating more (FP) and **OFA** missing more associations (FN). In light of this study, we use **OFA & LLaVA** to create pseudo-GT sentence-image relevance scores whenever GT information is not available. Note that the overhead of this computation does not affect the methods themselves, as it is used for evaluation only.

D. Design choices

In this section we recall and detail our default parameter setting. We use Open-CLIP [17] trained on LAION-2B [39] as our default visual-textual embedding space, but one could use other VLM models, such as BLIP [24], *etc.* To generate the GT sentence set \mathcal{S}_β^* , we use $\beta = o * \omega_\theta^{\text{std}}$, where $\omega_\theta^{\text{std}}$ is the standard deviation of ω_θ computed over \mathcal{X} with $o = 0.2$ as default value. We set the number of hard and easy clusters to $C = 15$ for large datasets (when we analyze the full set, namely urban scene segmentation and the unsupervised analyses on the NICO++ datasets) and to $C = 5$ for small sets, namely when we analyze the dataset for each class independently (per-class analyses of NICO++ and ImageNet). We set the number of retained sentences per cluster for all methods to $K = 3$.

In the unsupervised cases, we split \mathcal{X} according to $t_\phi^h = \phi_\theta^{\text{avg}} + a * \phi_\theta^{\text{std}}$ and $t_\phi^e = \phi_\theta^{\text{avg}} - a * \phi_\theta^{\text{std}}$, where ϕ_θ is the model’s output entropy and we set $a = 0.2$ as default value. In the per-class analysis using NICO++ datasets, we use class probabilities ρ_θ and split according to $t_\rho^h = \rho_\theta^{\text{avg}} - a * \rho_\theta^{\text{std}}$ and $t_\rho^e = \rho_\theta^{\text{avg}} - a * \rho_\theta^{\text{std}}$. For ImageNet, the splitting is done according to the ranking, with the hard set including both false positives (the GT class not ranked first) and false negatives (an image not labeled with the current class where the model ranked the current class as first)—as described in Appendix A.

E. Further qualitative analyses

First, we provide in Tab. 5 an extended version of Tab. 1. We show qualitative examples for ImageNet 1K using the pre-trained ViT-B16 model in Figs. 12 and 13, for NICO₊₊⁸⁵ in Fig. 14, and finally further examples obtained for the urban scene segmentation model on WD2 in Fig. 15. We conclude the section with Tab. 5 which is an extended version of Tab. 1 in the main paper.

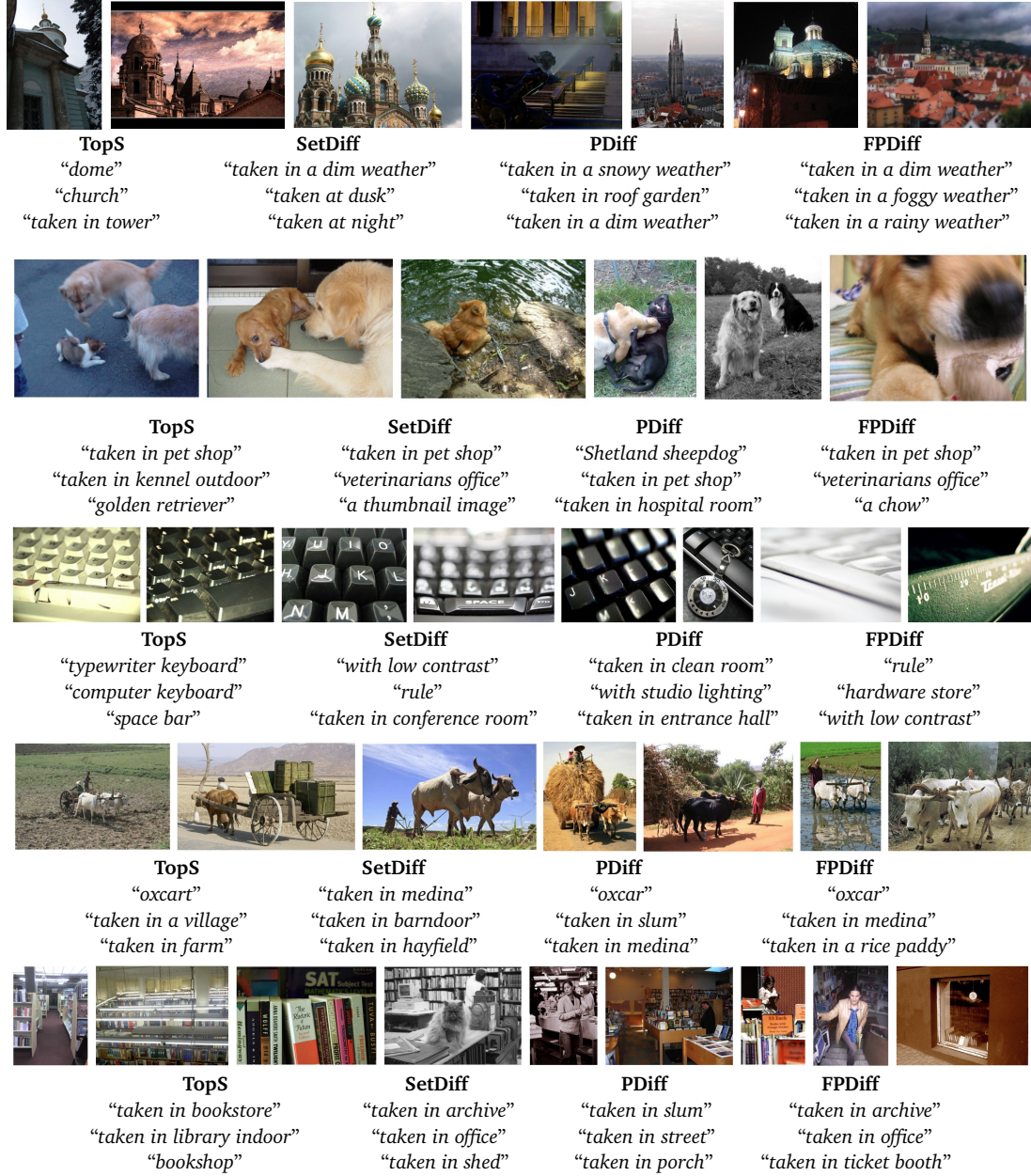


Figure 12: Hard clusters from ImageNet 1K validation set tested with the pre-trained ViT-B16 model. Here we show examples containing mainly false negative (images from the current class not recognized). From top to bottom we have the classes “church”, “golden retriever”, “computer keyboard”, “ox” and “bookshop”.



Figure 13: Hard clusters from ImageNet 1K validation set tested with the pre-trained Vit-B16 model. Here we show examples containing mainly false positive (images from other classes wrongly labeled with the current class name). From top to bottom we have the classes "red fox", "rock crab", "microwave", "cucumber" and "water snake".

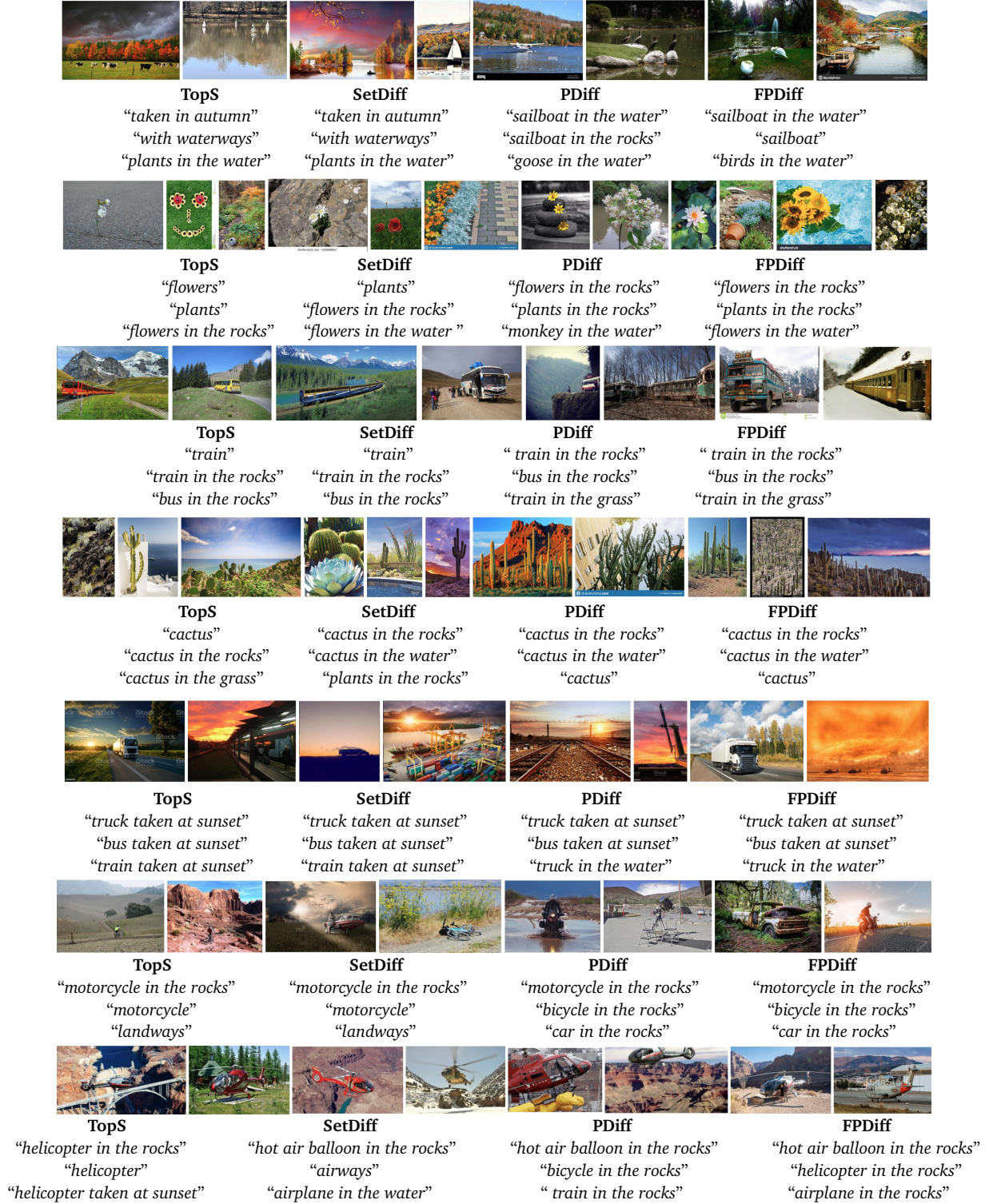


Figure 14: Seven out of 15 hard clusters from NICO₊₊⁸⁵ (unsupervised case) explained by different methods.

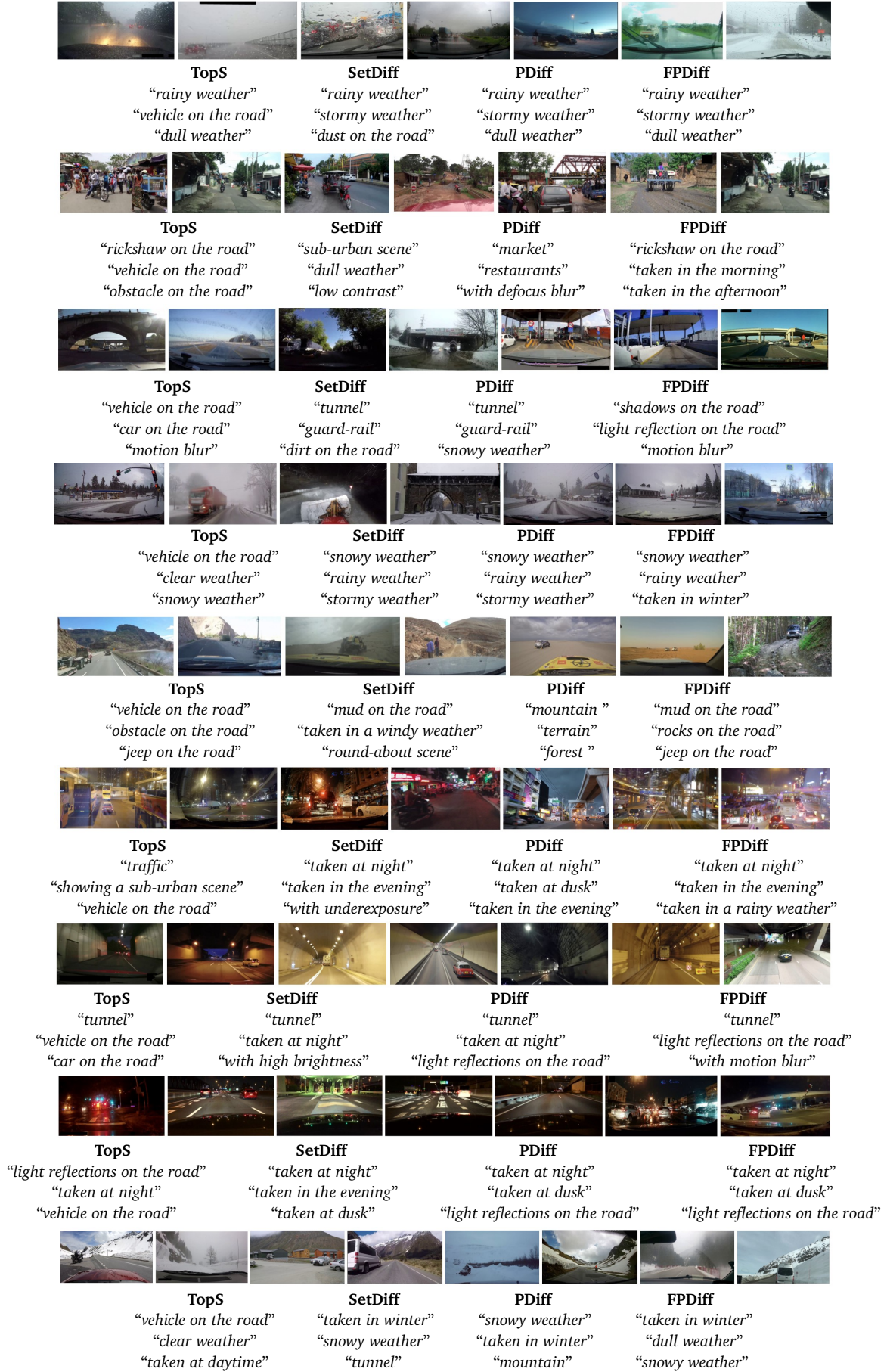


Figure 15: Nine out of 15 hard clusters from WD2 explained by different methods.

Table 5: Example sentences from the User-defined sentence set \mathcal{S} . For each sentence we show if it belongs to \mathcal{S}_β^* (obtained with $\alpha = .2$) and to $\mathcal{R}_\mathcal{S}$ for **TopS** (TS), **PDiff** (PD), **SetDiff** (SD) and **FPDiff** (FP) for the datasets WD2, IDD and ACDC. For \mathcal{S}_β^* , “✓” means $s_n \in \mathcal{S}_\beta^*$ and “✗” means $s_n \notin \mathcal{S}_\beta^*$ —namely, for that dataset the hardness score of s_n is below the required level. For the methods, “+”/“+” indicate that the sentence is in $\mathcal{R}_\mathcal{S}$, where “+” means true positive (i.e., the sentence is also in \mathcal{S}_β^*) while “+” means false positive. An empty space indicates that the sentence is not in the corresponding $\mathcal{R}_\mathcal{S}$. Note that the table is not complete as we omitted to show a few sentences that were not in any \mathcal{S}_β^* , semantically very similar to a sentences in the table with similar behaviour or retained by a single method for one dataset, but gives a very good overview of the set based results.

Sentences (<i>An image ...</i>)	WD2					IDD					ACDC				
	\mathcal{S}^*	TS	PD	SD	FP	\mathcal{S}^*	TS	PD	SD	FP	\mathcal{S}^*	TS	PD	SD	FP
“taken at night”	✓	+	+	+	+	✓		+	+	+	✓	+			
“taken in the evening”	✓		+	+	+	✓		+		+	✓	+			
“taken at dusk”	✓		+	+	+	✓		+	+	+	✓				
“taken at dawn”	✗		+			✓		+	+		✗				
“taken in a stormy weather”	✓		+	+	+	✗					✗				+
“taken in a foggy weather”	✓			+		✓					✗	+	+	+	+
“taken in a rainy weather”	✓	+	+		+	✓					✗	+	+		+
“taken in a snowy weather”	✓		+	+	+	✗					✗	+			
“taken in a windy weather”	✓	+	+	+	+	✗					✗		+		+
“taken in a dull weather”	✓	+	+	+	+	✗					✗	+	+	+	+
“taken in winter”	✓			+	+	✗					✗				+
“taken in autumn”	✗		+			✓					✗				
“with reflection on the road”	✓	+	+	+	+	✓			+		✓				+
“with shadows on the road”	✗				+	✗			+		✓			+	
“with water on the road”	✓	+				✗					✗			+	+
“with mud on the road”	✗			+	+	✗		+	+		✗				
“with branches on the road”	✓					✓			+	+	✗		+	+	+
“with traffic cone on the road”	✓					✓					✓		+	+	+
“with obstacle on the road”	✓	+			+	✗	+				✗				
“with road barrier on the road”	✗			+		✗			+	+	✓	+	+	+	+
“with rail track on the road”	✗					✓			+	+	✓	+	+	+	+
“with rocks on the road”	✗			+	+	✗					✗				
“showing a highway scene”	✗			+		✗			+	+	✗	+	+	+	+
“showing an industrial scene”	✓					✓					✗				
“showing construction site”	✗					✓		+	+	+	✗		+	+	
“showing sub-urban scene”	✗	+		+		✗	+			+	✓				
“showing agricultural field”	✗					✓					✗				
“showing a round-about”	✗					✗					✓				
“with rickshaw on the road”	✗	+	+	+	+	✗	+	+		+	✓		+		
“with motorbike on the road”	✗		+		+	✗				+	✓				+
“with bike on the road”	✗					✗			+	+	✗			+	
“with vehicle on the road”	✗	+				✗	+				✗	+	+	+	+
“with bus on the road”	✗					✗	+	+		+	✗			+	
“with tram on the road”	✗					✗			+		✗	+	+		+
“with jeep on the road”	✗	+		+	+	✗					✗				
“with animal on the road”	✗			+	+	✓			+	+	✗				
“with bird on the road”	✗					✓					✗				
“with people on the road”	✗	+			+	✗	+			+	✗		+		
“with crowded background”	✗					✓			+		✗				
“with crowded foreground”	✗					✗		+	+	+	✗				
“with motion blur”	✓	+	+		+	✓			+	+	✓		+		
“with overexposure”	✓					✗					✗				
“with underexposure”	✗			+	+	✗					✓			+	
“with low contrast”	✓					✗			+	+	✗			+	
“of a tunnel”	✓	+	+	+	+	✓		+			✓	+	+	+	+
“of fences”	✗					✗		+			✓		+		
“of guard-rail”	✗					✗					✗		+	+	+
“of a traffic jam”	✓					✓	+	+		+	✗				
“of a traffic”	✗	+				✗	+	+		+	✗		+		
“of traffic lights”	✓					✓					✗		+		
“of buildings”	✗		+			✗		+			✗		+		
“of a parking”	✗		+			✓		+	+	+	✗		+		
“of a mountain”	✗	+	+			✗					✗				